General Disclaimer

One or more of the Following Statements may affect this Document

- This document has been reproduced from the best copy furnished by the organizational source. It is being released in the interest of making available as much information as possible.

- This document may contain data, which exceeds the sheet parameters. It was furnished in this condition by the organizational source and is the best copy available.

- This document may contain tone-on-tone or color graphs, charts and/or pictures, which have been reproduced in black and white.

- This document is paginated as submitted by the original source.

- Portions of this document are not fully legible due to the historical nature of some of the material. However, it is the best reproduction available from the original submission.

Prepared for
GEORGE C. MARSHALL SPACE FLIGHT CENTER
Huntsville, Alabama

BER RESEARCH ENGINEERING BUREAU OF

ANTENNA ARRAYS: EFFICIENCY AND EFFICIENCY IMPROVEMENT THROUGH COMPENSATION

Technical Report No. 1
Contract NAS8-25894
October 1, 1970

by

Dr. James E. Dudgeon
Project Director
Department of Electrical Engineering

BER

COLLEGE OF ENGINEERING

UNIVERSITY OF ALABAMA

UNIVERSITY ALABAMA

University of Alabama
Bureau of Engineering Research
University, Alabama

ANTENNA ARRAYS: EFFICIENCY AND EFFICIENCY IMPROVEMENT THROUGH COMPENSATION

Technical Report No. 1
Contract NAS8-25894

Prepared by

Dr. James E. Dudgeon
Project Director
October 1, 1970

Submitted to

George C. Marshall Space Flight Center
National Aeronautics and Space Administration
Huntsville, Alabama

TABLE OF CONTENTS

CONTENTS (Continued)

LIST OF FIGURES

Figures (Cont'd) Title Page

ACKNOWLEDGEMENT

The author wishes to express his special appreciation to Messrs. G. Saunders, R. Mixon, D. O. Lowery, and J. W. Harper at George C. Marshall Space Flight Center for their valuable assistance and many helpful discussions.

ABSTRACT

The primary purpose of this report is to present and investigate design procedures for compensating the elements in a phased array antenna for impedance changes with scan angle. With proper compensation it is possible to improve the overall array efficiency and in many instances to increase the usable scan range for the array. Also included is a survey of the design results for scanned array antennas and a coverage of the factors affecting array efficiency changes with scan angle such as mutual coupling, element placement, surface wave coupling, and polarization. Two basic approaches to compensation for impedance variations with scan angle are detailed. The first considers the effects of structures which modify the array environment such as baffles and dielectric cover sheets. The other deals with methods which depend on behind-the-array circuitry for matching.

I. INTRODUCTION

As is well known, the variations of active element impedance with scan angle in phased arrays can seriously affect array efficiency. The primary objective of this report is to present methods to compensate for these impedance changes and thereby increase the usuable scan range for a given antenna array. The principal methods of compensation are presented in Chapter V, and the reader is immediately referred to that chapter if that is his sole interest. The rest of the report is intended as a survey which hopefully presents many of the important design considerations used in array theory in an easily accessible form. Special emphasis is placed on understanding what really influences array efficiency, and the resultant analysis separates the contributing factors into two levels. The first ignores the particular type of element and its mutual coupling and concentrates on the effects of element placement and spacing on efficiency. The second level goes deeper by including mutual coupling and element characteristics in the evaluation of array performance.

In most of compensation techniques developed in this paper, it is assumed that the system complexity is so great that it is necessary to utilize measured data from the original array or an array simulator as the basis for the matching. The two common ways to experimentally evaluate array operation are as follows:

(1) Passive Array Measurements One element (central) is excited with all others terminated in their generator impedances. Nulls or dips in patterns measured under this condition usually correspond to "blind"

spots to scan for the active array. For infinite arrays nulls are expected at such points, and for finite arrays the active array can be expected to have at best a pattern dip near these scan angles. Generally the 3 db bandwidth of the passive array element pattern is an approximate measure of the high efficiency scan range for the active array. In addition, coupling coefficients are defined and measured for the array in this state, and in Chapter IV it will be shown that these can be used to predict active array reflection coefficients and impedance behavior for different scan angles. The passive array measurements are easy-to-implement and provide considerable information about active array characteristics.

(2) Active Array Measurements In an active array measurement all elements are excited. Here not only pattern, but reflection coefficient and impedance can be measured directly. The trouble is that this method is much more cumbersome than the passive array measurement in that all of the elements have to be actively fed and properly phased at each different beam setting. As a consequence, it is not used as frequently as the passive array method, and it is not recommended for prototype arrays with a large number of elements.

Chapter II is a survey of design results for scanned array antennas having a uniform amplitude distribution across the elements with beam pointing accomplished by varying the progressive element phase shift. Included in this chapter are beamwidth and grating lobe effects. Linear, rectangular, and equilateral triangular lattices are treated.

Chatper III delves into element efficiency from the first level viewpoint previously defined to include such geometric effects as place-

ment and spacing. Some of the results presented here should prove especially useful to an array designer.

Chapter IV is an attempt to introduce and summarize some of the effects of scan angle on mutual coupling, impedance, and polarization in infinite arrays. An approximate formula is developed to give a qualitative estimation of impedance variations with scan angle, and some of the effects on impedance scan properties caused by certain array alterations are examined. Also included is a fairly exhaustive analysis of active array impedance and efficiency variations for an infinite linear array of short dipoles which allows for the mutual impedance and pattern effects of a real element. This analysis defines mutual coupling parameters, and it gives a good example of their application to active array problems where generator impedance effects must be included. Also in this chapter, the topic of surface waves is first introduced and related to possible degradation of the usable scan range to values below those expected from simple grating lobe considerations. As will be seen, this phenomenon severely affects the scan range of the dielectric sheet compensation method covered in Chapter V. The subject of surface waves is treated in great detail in Chapter V for a special array loading, however, in Chapter IV surface wave treatment is more general in that it is intuitively deduced and can be applied to any array surface.

As previously stated Chapter V covers the methods used to compensate for array impedance variations with scan angle. The approaches are divided into those which modify the array environment with such things as baffles, fences, or dielectric sheets and those which use behind-the-array circuitry for matching. Much work has been done to supplement the

work contained in the literature on these methods. As for the choice of method it will be seen that this is largely dictated by design requirements. The matching dielectric sheet technique is probably cheapest and simplest for compensating arrays of flush-mounted antenna elements, however, it lacks great precision so that extremely low VSWR's are not to be expected, and it is often limited by surface wave effects to usefulness over smaller scan ranges than the coupling element techniques. The matching circuit techniques treated in this chapter can all be considered variations of Hannan's scheme of coupling adjacent array positions with susceptive networks. Again this method offers a range of choices depending on the precision and scope of scan. Some efficiency improvement is obtained by using only pre-element matching networks, however, the more general method interconnects an element with its eight closest neighbors and is capable of achieving excellent match over fairly wide scans. Probably the main drawbacks of the connecting circuit method are its initial expense and the complexity of the design. Still, for arrays with a large number of elements using modular elements, it is likely that the necessary circuitry could be incorporated into the modules without significantly increasing the cost. Also included in this chapter is a procedure for realizing Hannan's connecting circuit match with the aid of a digital computer.

II. SUMMARY OF DESIGN RESULTS FOR SCANNED ARRAYS WITH UNIFORM AMPLITUDE ILLUMINATION

A. LINEAR ARRAYS[1] (Fig. 1)

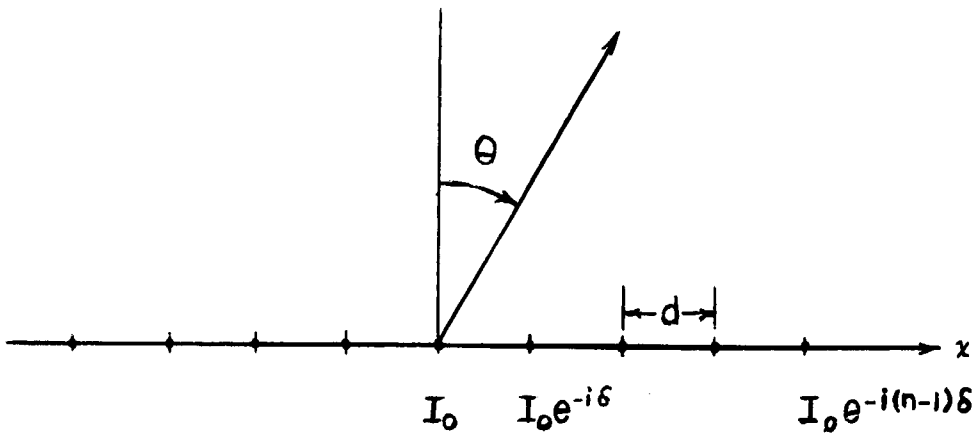

Fig. 1 Linear Array

Pattern Factor (N elements, uniform amplitude distribution, far-field pattern)

Normalized pattern factor

$$F_N = \frac{1}{N} \frac{\sin \frac{N}{(2)}\psi}{\sin (\frac{\psi}{2})} \qquad (2\text{-}1)$$

where $\psi = kd \sin \theta - \delta = kd \sin \theta - k_x d.$ (2-2)

d = element spacing

$k = 2\pi/\lambda.$

Main Beam

The beam maximum occurs when $\psi = 0$. Thus a beam maximum at $\theta = \theta_s$ requires

$$\delta = kd \sin \theta_s = k_x d = \text{progressive per element phase shift}$$
$$\theta_s = \text{beam scan angle}. \qquad (2\text{-}3)$$

From (2-2) it is seen that the progressive phase constant to direct the beam in the θ_s-direction is given by

$$k_x = k \sin \theta_s. \qquad (2\text{-}4)$$

Grating Lobes

These are main beam maximums which occur when the interelement spacings are such that $\psi = 0$ at angles other than $\theta = \theta_s$ in visible space ($| \sin \theta | \leq 1$)

$$\frac{\psi}{2} = \pm p\pi = \frac{\pi d}{\lambda} [\sin \theta - \sin (\theta_s)]$$

Manipulating the above it can be shown that grating lobes can be avoided in the scan range $| \theta | \leq \theta_m$ if

$$\frac{d}{\lambda} \leq \frac{1}{1 + | \sin \theta_m |} \qquad (2\text{-}5)$$

Obviously for $d \leq \lambda/2$ no grating lobes appear in visible space.

Half-Power Beamwidth (3 db beamwidth)

$$\theta_{\frac{1}{2}} = \text{half-power beamwidth} = \theta_2 - \theta_1 \qquad (2\text{-}6)$$

where $F_n(\theta_i) = .707\, F_N(\theta_s) \qquad i = 1, 2.$

Written out this becomes

$$.707 = \frac{1}{N} \frac{\sin\left[\frac{N\psi_i}{2}\right]}{\sin\left(\psi_i/2\right)} \qquad (2\text{-}7)$$

For large N and scan angles close to Θ_1 or Θ_2 Eq. 2-7 is approximately

$$\frac{\sin\left[\frac{(N\ \psi_i)}{2}\right]}{N \sin\left(\frac{\psi_i}{2}\right)} = .707 \simeq \frac{\sin\left[\frac{(N\ \psi_i)}{2}\right]}{\frac{(N\ \psi_i)}{2}}$$

Solving the above gives the half-power points at $\frac{N\ \psi_i}{2} = \pm\ 1.39$.

Thus $\psi = kd\ (\sin\theta_i - \sin\theta_s) = \pm\ \frac{2.78}{N}$

$$\sin\theta_i = \sin\theta_s \pm \frac{2.78}{kdN}$$

yielding for a linear array

$$\theta_{1/2} = \text{half-power beamwidth} = \sin^{-1}\left[\sin\theta_s + \frac{.443\lambda}{L}\right]$$

$$- \sin^{-1}\left[\sin\theta_s - \frac{.443\lambda}{L}\right] \qquad (2\text{-}8)$$

where θ_s = scan angle

$L = Nd$ = array length + d

N = number of elements

Common Special Cases

(a) Broadside, $\theta_s = 0°$

$$\Theta_{\frac{1}{2}} = 2 \sin^{-1} \left[\frac{.443\ \lambda}{L} \right] \qquad (2\text{-}9)$$

(b) Broadside, with N large and $d = \lambda/2$ (optimum spacing for a linear array)

$$\Theta_{\frac{1}{2}} = 2 \sin^{-1} \left[\frac{.886}{N} \right] \simeq \frac{1.772}{N} \text{ (radians)}$$

$$\simeq \frac{101.8}{N} \text{ (degrees)} . \qquad (2\text{-}10)$$

Directivity

$$D = \frac{4\ |F_n|^2}{\int\int |F_n|^2\ d\Omega} = \frac{2\ \dfrac{\sin^2(N\psi/2)}{\sin^2(\psi/2)}}{\displaystyle\int_{-\pi}^{\pi} \frac{\sin^2(N\psi/2)}{\sin^2(\psi/2)}\ d\Omega}$$

$$D_N = \frac{1}{1 + \dfrac{2}{N^2} \displaystyle\sum_{1}^{N-1} (N-m)\ \frac{\sin\ (m\ k\ d)}{mkd}} \qquad (2\text{-}11)$$

Efficiency

The maximum theoretical efficiency for a linear array of "ideal" radiating elements as a function of element spacing is shown in Fig. 2 below.

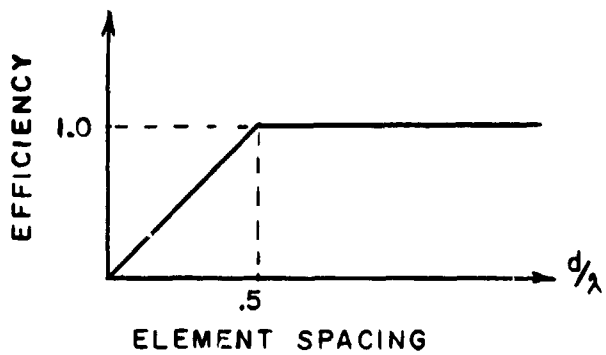

$\eta = \frac{2d}{\lambda}$ for $d \leq \lambda/2$

$\eta = 1$ for $d \geq \lambda/2$

Fig. 2 Maximum Efficiency of a Linear Array

Comparing the above with the condition that $d \leq \lambda/2$ for elimination of grating lobes in visible space, it is seen that $d = 0.5\ \lambda$ is an optimum choice, at least for the idealized case. The derivation of the above plot and a far more thorough treatment of both linear and planar array efficiencies will be covered in a later chapter. The influence on element efficiency of using a physical element instead of an ideal one is shown in a subsequent analysis of an infinite linear array of elementary dipoles.

B. PLANAR ARRAYS

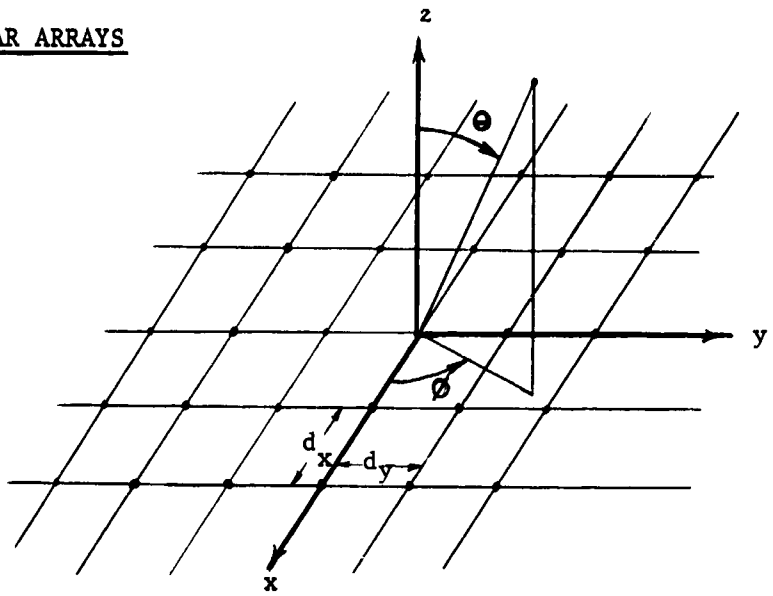

Fig. 3 Planar Array

The lattice points in a general planar array with parallelogram cells are given by

$$\bar{P}_{mn} = m\,\bar{a}_1 + n\,\bar{a}_2$$

For $\bar{a}_1 = \bar{a}_x$ and $\bar{a}_2 = \bar{a}_y$, a rectangular grid such as shown in Fig. 3 is obtained.

Pattern Array Factor (M x N array, rectangular grid, uniform amplitude distribution, far-field)

$$F(\theta,\phi) = \frac{1}{MN} \frac{\sin\left[\frac{M}{2}(k\,d_x \sin\theta\cos\phi - \delta_x)\right]}{\sin\left[\frac{1}{2}(k\,d_x \sin\theta\cos\phi - \delta_x)\right]} \frac{\sin\left[\frac{1}{2}(k\,d_y \sin\theta\sin\phi - \delta_y)\right]}{\sin\left[\frac{1}{2}(k\,d_y \sin\theta\sin\phi - \delta_y)\right]} \qquad (2\text{-}12)$$

Phase Increments to Point the Beam in the (θ_s,ϕ_s) Direction

The main beam maximum occurs at (θ_s,ϕ_s) if

$$\delta_x = k\, d_x \sin\theta_s \cos\phi_s$$

$$\delta_y = k\, d_y \sin\theta_s \sin\phi_s \,. \qquad (2\text{-}13)$$

Grating Lobes

1. Rectangular grid (Fig. 4(a))

   For conical scan over the range $\theta \leq \theta_m$ and $0 \leq \phi \leq 2\pi$ the grating lobe maximum can be avoided if

$$\frac{d}{\lambda} \leq \frac{1}{1 + |\sin\theta_{max}|} \qquad (2\text{-}14)$$

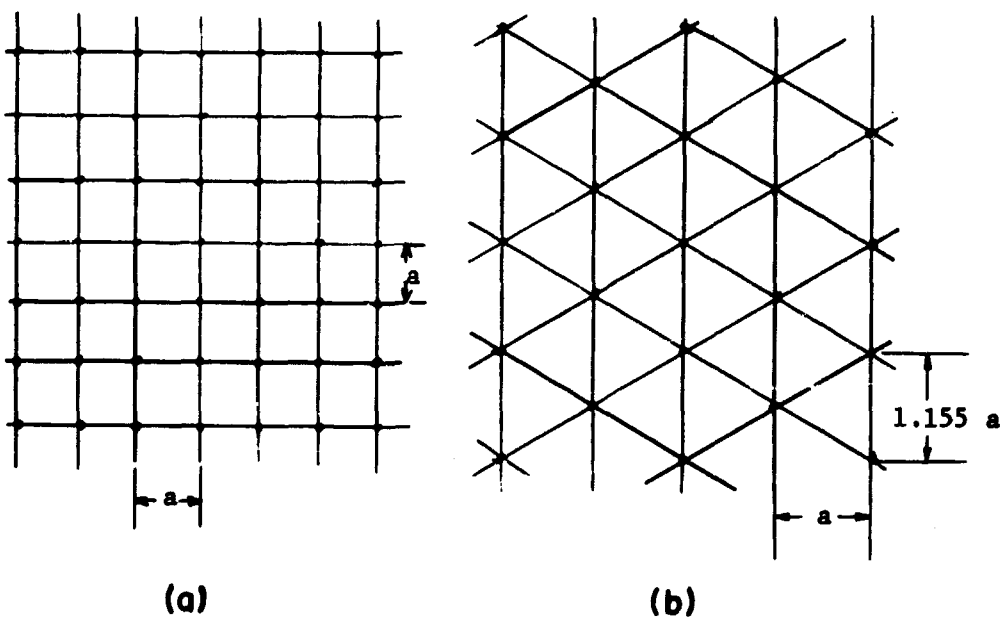

Fig. 4 Square and Equilateral Triangular Grids

The author can show for $N \geq 10$ that a better grating lobe condition is

$$\frac{d}{\lambda} \leq \frac{1 - \frac{.815}{N}}{1 + |\sin\theta_{max}|} . \qquad (2\text{-}15)$$

The condition in (2-14) is such that the grating lobe produces a sidelobe of nearly the amplitude of the main beam when the beam is aimed in the θ_{max}-direction. Equation 2-15, on the other hand, limits the grating sidelobe to a maximum amplitude in real space equal to the first sidelobe level.

2. Equilateral Triangular Grid (Fig. 5)

This configuration is optimum in the sense that the number of elements is minimized for a given area designed to have no grating lobes in an allowed conical scan region about broadside. For a given effective array aperture with maximum interelement spacing to suppress grating lobes, the total areas are

(a) Square grid: $A_1 = N_1^2 a^2$

(b) Equilateral triangular grid: $A_2 = N_2^2\ 1.155\ a^2 = \frac{2}{\sqrt{3}} N_2^2 a^2$.

Since $A_2 = A_1$, $N_2^2 = \frac{\sqrt{3}}{2} N_1^2 = .866\ N_1^2$, and hence for the same effective areas, the equilateral triangular grid array yields a 13.4% savings [2] in the number of elements.

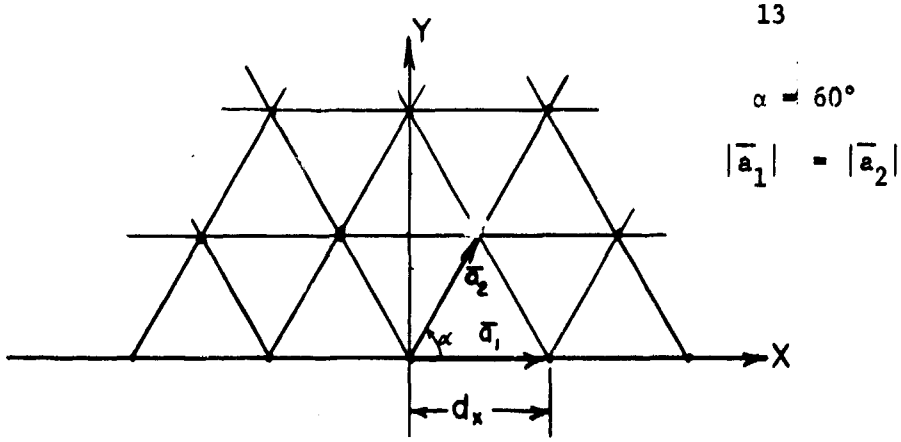

Fig. 5 Equilateral Triangular Grid Geometry

For the scanning range $|\theta| \leq \theta_m$ and $0 \leq \phi \leq 2\pi$

where θ_m = maximum scan angle, the spacing conditions necessary to eliminate grating lobes and use the minimum number of elements are

$$d = |a_1| = |a_2| \leq \frac{2}{\sqrt{3}} \frac{\lambda}{1 + \sin \theta_m} = \frac{1.155\lambda}{1 + \sin \theta_m} , \quad (2\text{-}16)$$

or, as in (2-15), limiting the amplitude of the grating sidelobe to that of the first sidelobe

$$\frac{d}{\lambda} \leq \frac{1.155 - \frac{.815}{N}}{1 + \sin \theta_m} . \quad (2\text{-}17)$$

For N large

$$\bar{a}_1 = \bar{a}_x \frac{2\lambda}{\sqrt{3}\,(1 + \sin \theta_m)} = \frac{1.155\lambda\, \bar{a}_x}{1 + \sin \theta_m} \quad (2\text{-}18)$$

$$\bar{a}_2 = \frac{2\lambda}{\sqrt{3}\,(1 + \sin \theta_m)} [\bar{a}_x \cos 60° + \bar{a}_y \sin 60°]. \quad (2\text{-}19)$$

From the above

$$d_x \leq \frac{1.155\lambda}{1 + \sin \theta_m} \tag{2-20}$$

$$d_y \leq \frac{\lambda}{1 + \sin \theta_m} \tag{2-21}$$

Examples (assuming N in Eq. 2-17 is very large):

$a_1\ (45°) = d_x\ (45°) \leq .678\lambda \rightarrow 45°$ scan

$a_1\ (60°) = d_x\ (60°) \leq .62\lambda \rightarrow 60°$ scan

$a_1\ (90°) = d_x\ (90°) \leq .578\lambda \rightarrow 90°$ scan

Obviously complete visible scan is possible if

$d_x \leq .578\lambda$

$d_y \leq .5\lambda$.

Area of parallelogram = $A_E = \bar{a}_1 \times \bar{a}_2 = |a_1|\ |a_2|$ sin 60° =

$$A_E = \frac{2}{\sqrt{3}} \quad \frac{\lambda^2}{(1 + \sin \theta_m)^2}$$

$$A_E = \frac{1.155\ \lambda^2}{(1 + \sin \theta_m)^2} \tag{2-22}$$

III. ELEMENT EFFICIENCY

In this chapter the effects of array geometry and interelement spacing on element efficiency will be examined. The resultant efficiencies are theoretical maximums obtained by postulating and using "ideal" radiating elements in infinite arrays. The geometries considered are linear, planar with a rectangular grid, planar with a triangular grid, and planar with an arbitrary parallelogram grid.

As is well known, efficiency limits are affected by the trade-off between grating lobe suppression and mutual coupling in phased arrays used for scanning. For regularly spaced and uniformly illuminated array elements, grating lobes can be eliminated by keeping the element spacings below certain values. However, problems arise because decreasing element spacings normally increases the mutual coupling between elements, leading to impedance mismatches and consequent power reflection and efficiency losses that vary with scan angle. This section will initially ignore impedance effects and concentrate on how the array geometry affects the amount of power actually radiated into visible space as compared with the power which is available from the array. As will be seen, even this restricted definition of efficiency puts conflicting demands on element spacing in that 100% efficiency typically requires spacings greater than the maximum allowed to avoid grating lobes.

A. Definitions

In this analysis the following definitions are used: [3]

(1) Element efficiency

$$\eta = \frac{\text{Power Radiated}}{\text{Power Available}} = 1 - \frac{\text{Power Reflected}}{\text{Power Available}} \qquad (3\text{-}1)$$

(2) Directive gain

$$g_d(\theta,\phi) = \frac{4\pi\ U\ (\theta,\phi)}{\iint U\ d\Omega} = \frac{4\pi U(\theta,\phi)}{\text{Power Radiated}} \qquad (3\text{-}2)$$

where $U(\theta,\phi)$ = radiation intensity and $d\Omega$ = differential solid angle.

(3) Realized gain

$$g_r(\theta,\phi) = \frac{4\pi\ U\ (\theta,\phi)}{\text{Power Available}} = \eta\ g_d \qquad (3\text{-}3)$$

(4) Efficiency in terms of reflection coefficient

$$\eta = 1 - \frac{1}{\pi^2} \int_0^{\pi} \int_0^{\pi} |\Gamma(\alpha_1,\alpha_2)|^2\ d\alpha_1\ d\alpha_2 \qquad (3\text{-}4)$$

where

Γ = reflection coefficient

α_1,α_2 = orthogonal phasing terms

(5) An <u>ideal element</u> is one whose

(a) element pattern has no grating lobes in the square $|\alpha_1| < \pi$ and $|\alpha_2| < \pi$ for the passive array environment.

(b) reflection coefficient is zero ($\Gamma = 0$) for all real angles of scan for the main beam in the active array configuration.

B. Linear Arrays (Fig. 6)

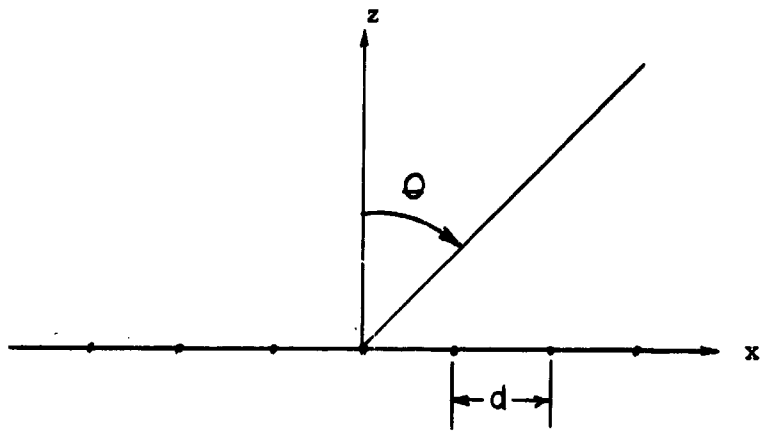

Fig. 6 Linear Array Geometry

Here

$$\eta = 1 - \frac{1}{\pi} \int_0^{\pi} |\Gamma(\alpha)|^2 \quad d\alpha \tag{3-5}$$

where

$$\alpha = kd \sin\theta = \frac{2\pi d}{\lambda} \sin\theta \ .$$

From the definition of an ideal element

$$|\Gamma| = 0 \quad \text{visible region} \quad (|\sin\theta| \leq 1)$$

$$|\Gamma| = 1 \quad \text{invisible region} \quad (|\sin\theta| > 1) \ .$$

Therefore for $d < \lambda/2$

$$\Gamma(\alpha) = 0 \text{ for } 0 \leq \alpha \leq (2\pi \ d/\lambda)$$

$$= 1 \text{ for } (2\pi \ d/\lambda) < \alpha < \pi \ ,$$

and hence

$$\eta = 1 - \frac{1}{\pi}\left(\pi - \frac{2\pi d}{\lambda}\right) = 2\, d/\lambda \text{ for } d < \lambda/2$$

$$= 1 \text{ for } d \geq \lambda/2 \qquad (3\text{-}6)$$

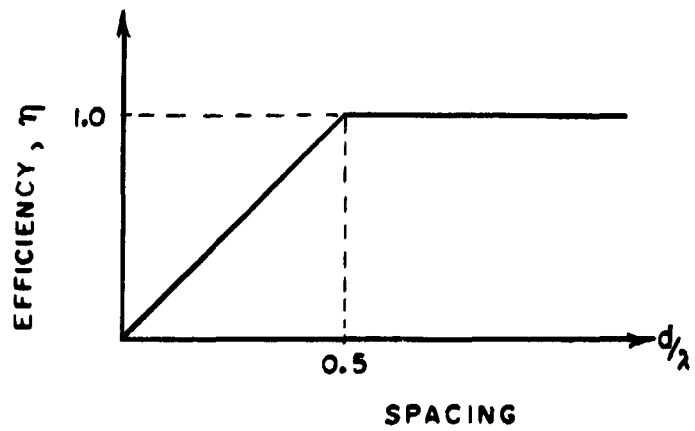

Fig. 7 Ideal Element Efficiency for a Linear Array

C. Rectangular Grid Arrays (Fig. 8)

Consider an infinite rectangular array in direction cosine space

$$v_1 = \cos \gamma_x = \sin \theta \cos \phi$$

$$v_2 = \cos \gamma_y = \sin \theta \sin \phi \qquad (3\text{-}7)$$

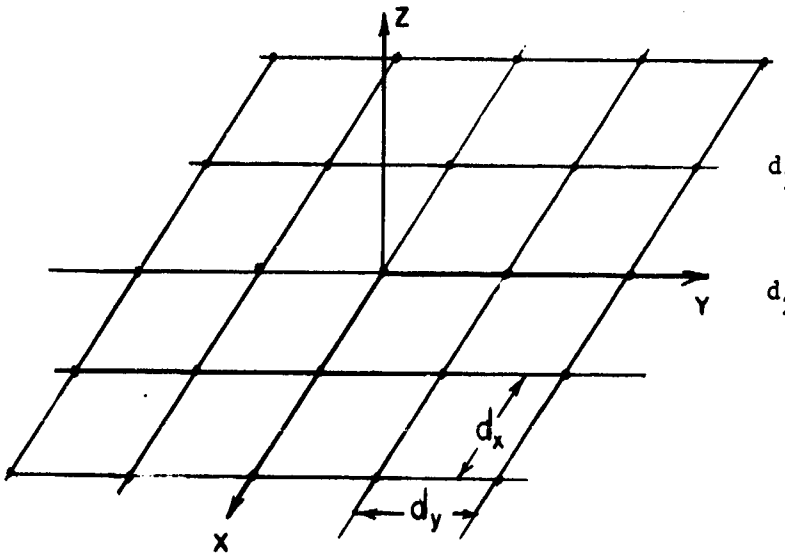

Fig. 8 Rectangular Grid

Then

$$\alpha_1 = k\, d_x\, v_1 = 2\pi\, d_1 \sin\theta \cos\phi$$

$$\alpha_2 = k\, d_y\, v_2 = 2\pi\, d_2 \sin\theta \sin\phi \qquad (3\text{-}8)$$

and

$$v_1 = \frac{\alpha_1}{2\pi\, d_1}$$

$$v_2 = \frac{\alpha_2}{2\pi\, d_2} \qquad (3\text{-}9)$$

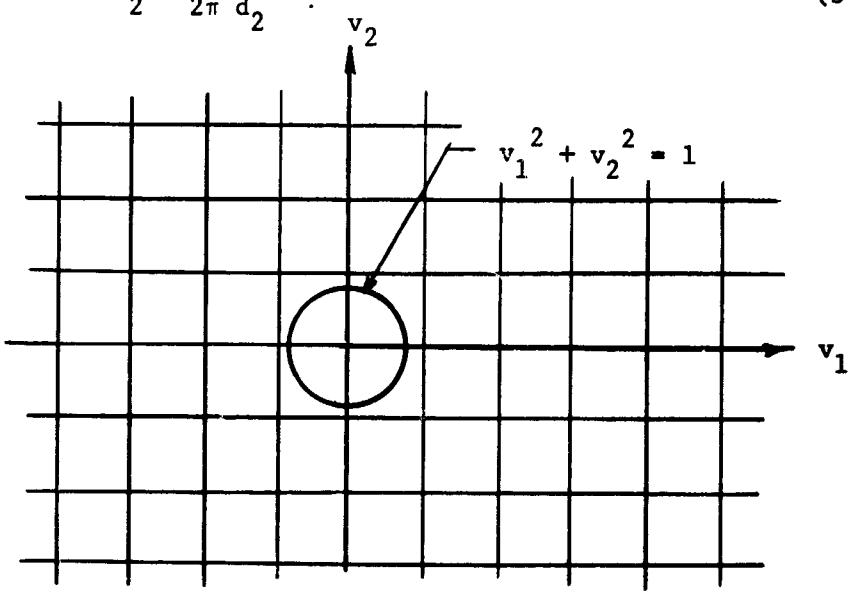

Fig. 9 Direction Cosine Space

The invisible-visible region boundary is the circle

$$v_1^2 + v_2^2 = 1 \quad . \tag{3-10}$$

Transforming to the α_1 α_2 plane produces an ellipse (Fig. 10)

$$\left[\frac{\alpha_1}{2\pi\ d_1}\right]^2 + \left[\frac{\alpha_2}{2\pi\ d_2}\right]^2 = 1 \tag{3-11}$$

with intercepts at $\alpha_1 = \pm\ 2\pi\ d_1$ and $\alpha_2 = \pm\ 2\pi\ d_2$.

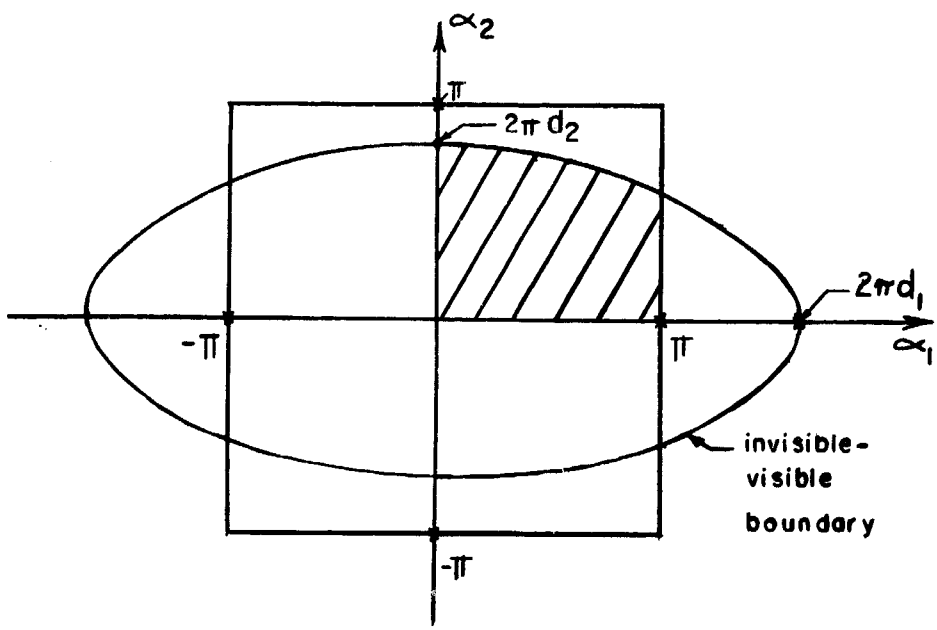

Fig 10 α_1 α_2 or Phase Space

Noting that

$$\eta = 1 - \frac{1}{\pi^2} \int_0^{\pi} \int_0^{\pi} |\Gamma(\alpha_1, \alpha_2)|^2\ d\alpha_1,\ d\alpha_2 \tag{3-12}$$

and

$\Gamma(\alpha_1, \alpha_2) = 0$ inside the ellipse in phase space (See Fig. 10)

$= 1$ outside the ellipse,

it follows that

$$\pi^2 \eta = \pi^2 - \int_0^{\pi} \int_0^{\pi} |\Gamma|^2 \, d\alpha_1 \, d\alpha_2$$

is numerically equal to the area common to the ellipse and the square $0 < \alpha_1 < \pi$ and $0 < \alpha_2 < \pi$ (shown shaded in Fig. 10).

Results:

(1) For small element spacing (d_1 and $d_2 \leq 0.5$),

$$\eta = \pi \, d_1 d_2$$

(2) For sufficiently large spacings ($d_1 > 0.5$ and $d_2 > \frac{1}{2\sqrt{1 - (\frac{1}{2d_1})^2}}$),

$$\eta = 1$$

(3) For $d_2 > 0.5$ and

$d_1 \leq 0.5$,

$$\eta = 2 \, d_1 \sqrt{1 - (\tfrac{1}{2d_2})^2} + 2 \, d_1 d_2 \left\{ \pi/2 - \sin^{-1} \sqrt{1 - (\tfrac{1}{2d_2})^2} - \tfrac{1}{2d_2} \sqrt{1 - (\tfrac{1}{2d_2})^2} \right\}$$

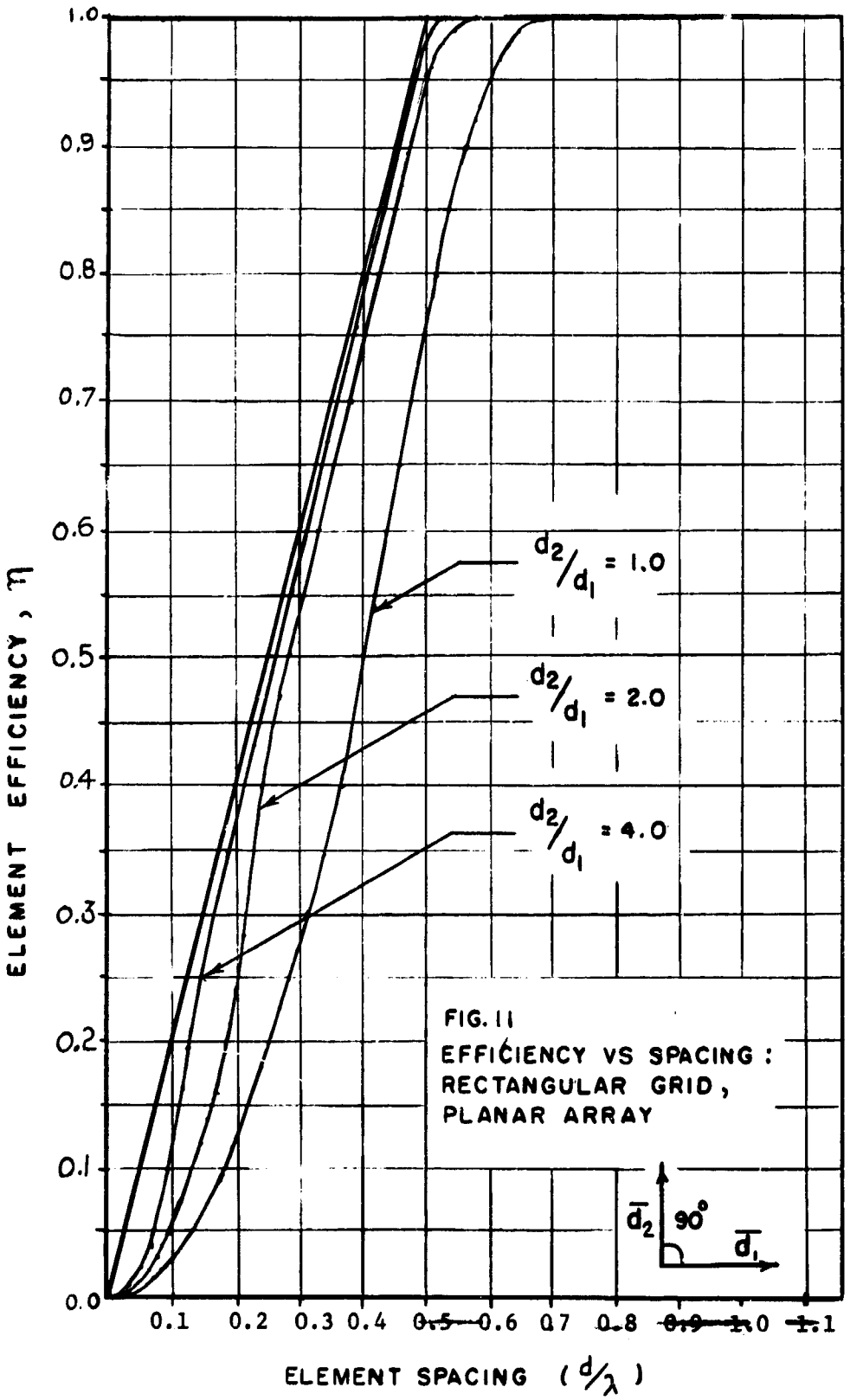

FIG. 11
EFFICIENCY VS SPACING : RECTANGULAR GRID, PLANAR ARRAY

(4) For $.5 < d_1 < .707$ and

$$.5 < d_2 < \frac{1}{2\sqrt{1 - (\frac{1}{2d_2})^2}} ,$$

$$\eta = 2d_1\sqrt{1 - (\frac{1}{2d_2})^2} + 2d_1 d_2 \{ \frac{1}{2d_1}\sqrt{1 - (\frac{1}{2d_1})^2} - \frac{1}{2d_2}\sqrt{1 - (\frac{1}{2d_2})^2}$$

$$+ \sin^{-1}(\frac{1}{2d_1}) - \sin^{-1}\sqrt{1 - (\frac{1}{2d_2})^2} \}$$

The results for several different ratios d_2/d_1 are shown plotted in Fig. 11.

D. General Parallelogram Lattice (Fig. 12)

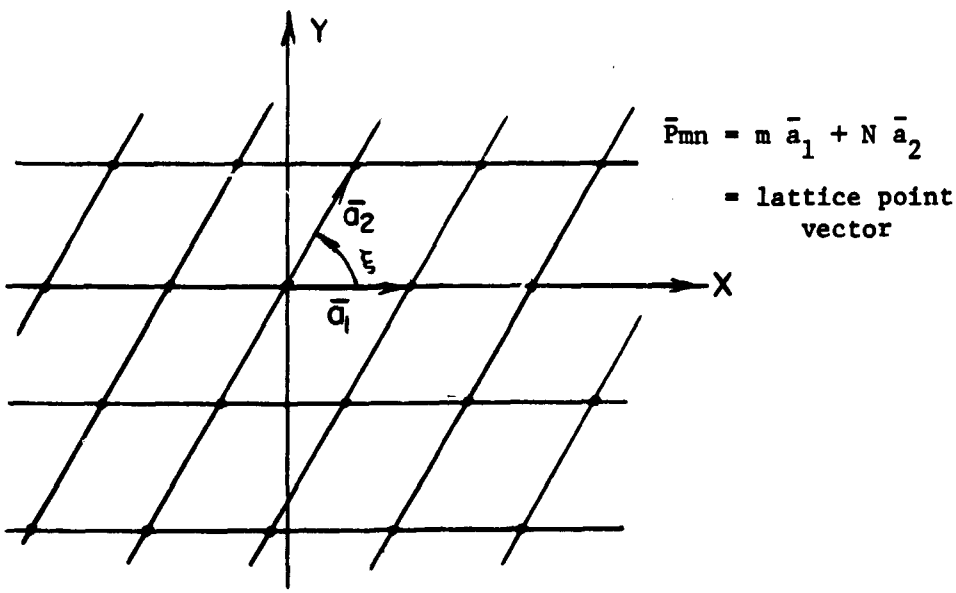

Fig. 12 Parallelogram lattice

* All distances are expressed as fractions of free space wavelength.

U-space is defined by the transformation

$$v_1 = \sin\theta \cos\phi = U_1/a_1$$

$$v_2 = \sin\theta \sin\phi = \frac{-U_1 \cos\xi}{a_1 \sin\xi} + \frac{U_2}{a_2 \sin\xi} \quad (3\text{-}13)$$

Substituting the above in the visible-invisible region boundary equation

$$v_1^2 + v_2^2 = 1$$

produces the ellipse

$$\left[\frac{U_1}{a_1}\right]^2 + \left[\frac{-U_1 \cos\xi}{a_1 \sin\xi} + \frac{U_2}{a_2 \sin\xi}\right]^2 = 1 \quad (3\text{-}14)$$

in U-space. Kahn [3] shows that in U-space for ideal elements the efficiency is equal to the area common to the invisible-visible boundary ellipse and a unit square. The equivalent area is shown shaded in Fig. 13 below.

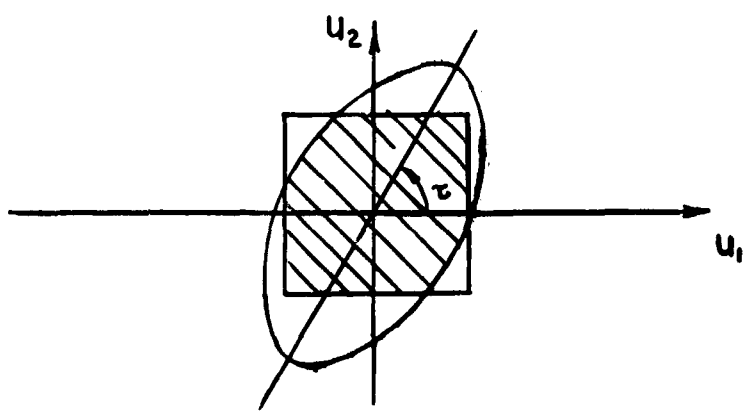

Fig. 13 U-space

The ellipse has:

$$\text{TILT ANGLE} \quad \tau = \frac{1}{2}\tan^{-1}\left[\frac{2\,a_1\,a_2\cos\xi}{a_1^{\,2} - a_2^{\,2}}\right] \tag{3-15}$$

$$\text{AXIAL RATIO} \quad AR = \tan\tau\,\frac{a_2\sin\xi}{a_1\tan\tau - a_2\cos\xi} \tag{3-16}$$

$$\text{INTERCEPTS} \quad U_1 = 0,\ U_2 = a_2\sin\xi$$
$$U_2 = 0,\ U_1 = a_1\sin\xi \quad . \tag{3-17}$$

Equilateral Triangular Grid

This important special case has $a_1 = a_2 = a$ and $\xi = 60°$. From the above

$$\tau = \pi/4 \text{ or } 45°$$
$$AR = \sqrt{3}$$
$$\text{intercepts:} \quad U_1 = 0,\ U_2 = 0.866a$$
$$U_2 = 0,\ U_1 = 0.866a,$$

and the appropriate boundaries in U-space are sketched below.

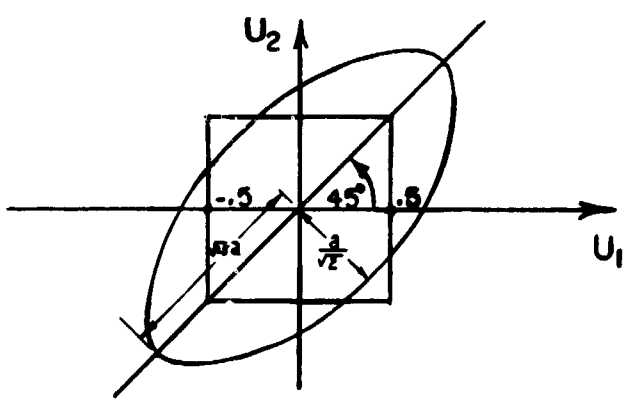

Fig. 14 U-space for an Equilateral Triangular Grid

Calculations for the equilateral triangular grid show that for

(1) $a \leq 0.5, \quad \eta = \frac{\pi a^2 \sqrt{3}}{2}$

(2) $0.5 < a < 1/\sqrt{3} = 0.5773,$

$$\eta = .75R + \sqrt{3}\, a^2 \left[\frac{1-R}{4a} \sqrt{1-\left(\frac{1-R}{4a}\right)^2} - \frac{1+R}{4a} \sqrt{1-\left(\frac{1+R}{4a}\right)^2} + \frac{\pi}{2} + \sin^{-1}\left[\frac{1-R}{4a}\right] - \sin^{-1}\left[\frac{1+R}{4a}\right] \right]$$

where $R = \sqrt{12a^2 - 3}$

(3) $1/\sqrt{3} \leq a < 1.0,$

$$\eta = \frac{1+R}{2} - \frac{(1+R)^2}{16} + \sqrt{3}\, a^2 \left[\frac{\pi}{2} - \left(\frac{1+R}{4a}\right)\sqrt{1-\left(\frac{1+R}{4a}\right)^2} - \sin^{-1}\left(\frac{1+R}{4a}\right)\right]$$

(4) $a \leq 1.0,$

$$\eta = 1.0$$

and the results are plotted in Fig. 15.

Kahn [3] has worked out several other cases which might prove useful, and these are presented in Figs. 16 and 17 below. Figure 16 shows the effect on efficiency of changing the sidelength ratio, a_2/a_1, on a 60° parallelogram lattice. Note that the commonly used equilateral case where $a_2 = a_1$ is in a sense worst from an efficiency standpoint. In Fig. 17 the corner angle of a rhombic grid has been varied, and it is observed that for a given element spacing, efficiency increases as the angle approaches 90°.

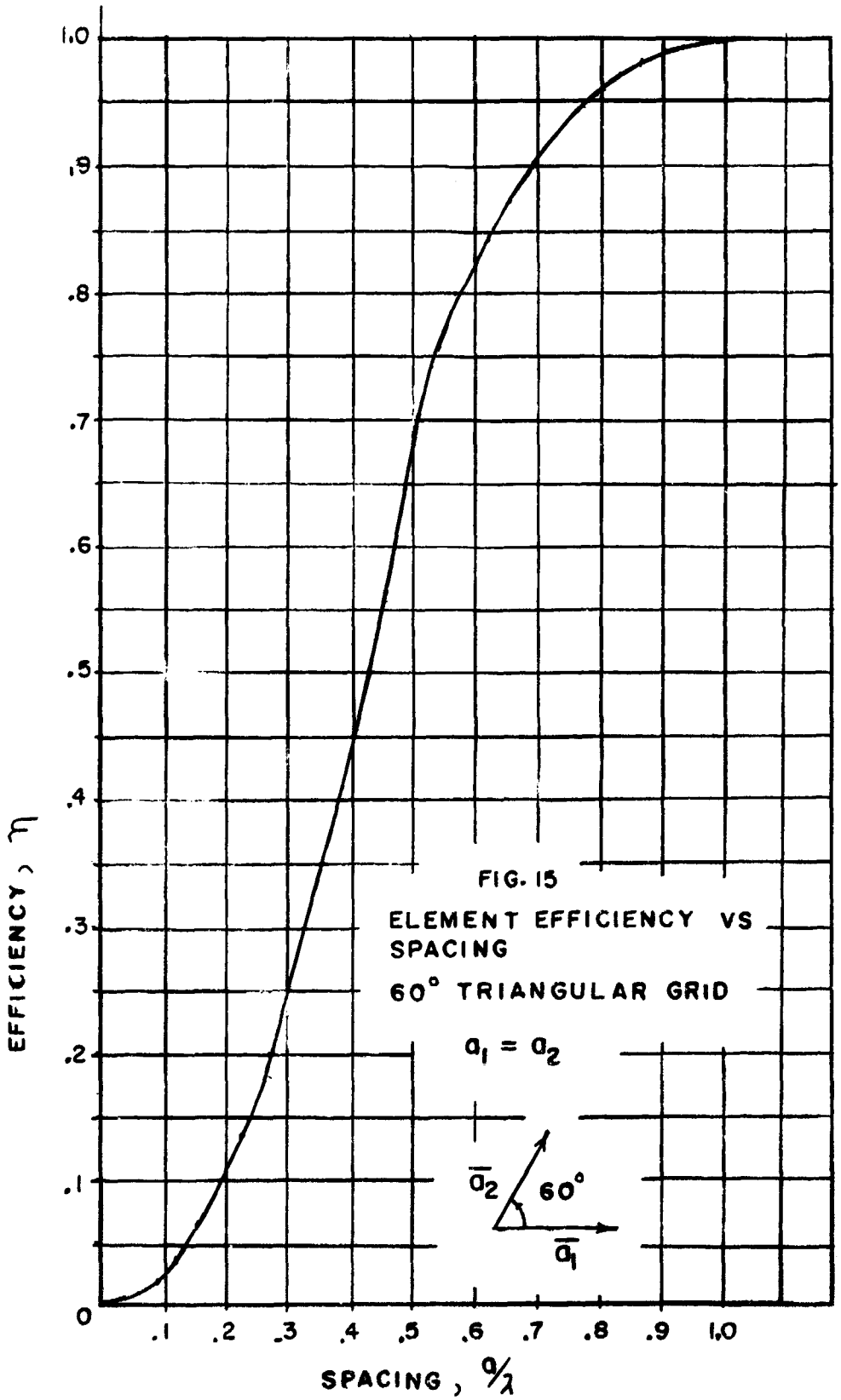
1.0
.9
.8
.7
.6
.5
.4
.3
.2
.1
0
EFFICIENCY, η
.1
.2
.3
.4
.5
.6
.7
.8
.9
1.0
SPACING, a/λ
FIG. 15
ELEMENT EFFICIENCY VS SPACING
60° TRIANGULAR GRID
a1 = a2
a2
60°
a1

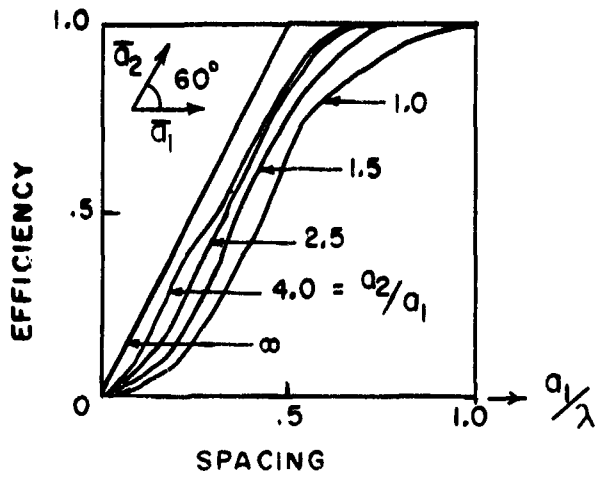

Fig. 16 Effect of Sidelength Ratio in a 60° Parallelogram Lattice

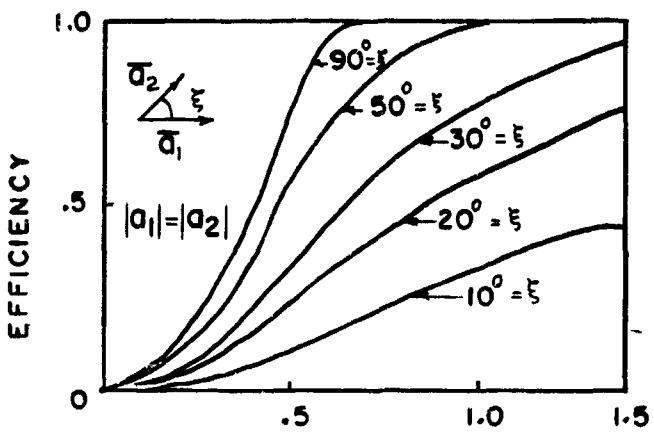

Fig. 17 Effect of Corner Angle in a Rhombic Lattice

Some sample calculations using the information in Figs. 11, 15, 16 and 17 which might prove interesting are given by the following examples:

(1) Square grid - 100% efficiency requires $d_1 = d_2 = \lambda/\sqrt{2} = 0.707\lambda$; maximum scan with grating lobe suppression

$$.707\lambda = \frac{1}{1 + \sin\theta_m} \rightarrow \theta_m \simeq 24.5° \text{ for 100\% efficiency}$$

(2) Equilateral triangular grid - 100% efficiency requires $a = \lambda$;

maximum scan without grating lobe $\rightarrow \frac{a_1}{\lambda} = 1.155/(1+\sin\theta_m)$

$\rightarrow \theta_m \simeq 9°$ for 100% efficiency

(3) 60° scan, square grid -

$d_x = d_y = (1.0/1.866)\lambda = 0.536\lambda$;

from Fig. 11, $\eta_{max} \simeq 0.85$

(4) 60° scan, equilateral triangular grid -

$d_x = a_1 = a_2 = .62\lambda$;

from Fig. 15, $\eta_{max} = 0.8435$

(5) 90° scan, square grid -

$d_x = d_y = 0.5\lambda$;

from Fig. 11, $\eta_{max} = 0.785$

(6) 90° scan, equilateral triangular grid -

$d_x = a_1 = a_2 = 0.5773\lambda$;

from Fig. 15, $\eta_{max} = 0.802$.

IV. EFFECTS OF SCAN ANGLE ON IMPEDANCE, MUTUAL COUPLING, AND POLARIZATION IN INFINITE ARRAYS.

The aim of this chapter is to introduce some of the terminology, analysis techniques, and difficulties associated with impedance and mutual coupling in scanned arrays. The early portion of the chapter contains some graphical results and a few formulas taken from the literature which are intended to give a qualitative feel for the behavior expected for array impedance variations with scan angle. Included are graphs showing special examples of the effects on impedance of ground planes, grating lobes, and element spacing. The primary literature sources for these results are Hansen[4] and Allen and Diamond [5] and these references are recommended for more comprehensive treatments and extensive bibliographies on the subject. Once some of the qualitative array effects are known, the active impedance and efficiency of an infinite linear array of elementary dipoles are calculated. The details of one of the common techniques for analyzing infinite arrays are illustrated by this application. In addition, this chapter contains an introduction to the troublesome effects of coupling waves which often produce gain losses at scan angles prior to grating lobe effects. Lastly, a qualitative summary of some of the factors that influence the polarization characteristics of a scanned array is given.

A. Approximate Impedance (or Admittance) Variations with Scan Angle

In this analysis it is assumed that the arrays are infinite or large enough to approximate the behavior of an infinite array, and hence, the method of periodic unit cells [6] may be used for calculations. By look-

ing at an array as an infinite sequence of periodic cells, it is possible to obtain an approximate formula for scan dependent impedance variations from geometric and physical considerations. For a beam streered in the θ-direction the periodic cells are aligned as shown in Fig. 18. Note that the results to be obtained are especially representative of arrays of

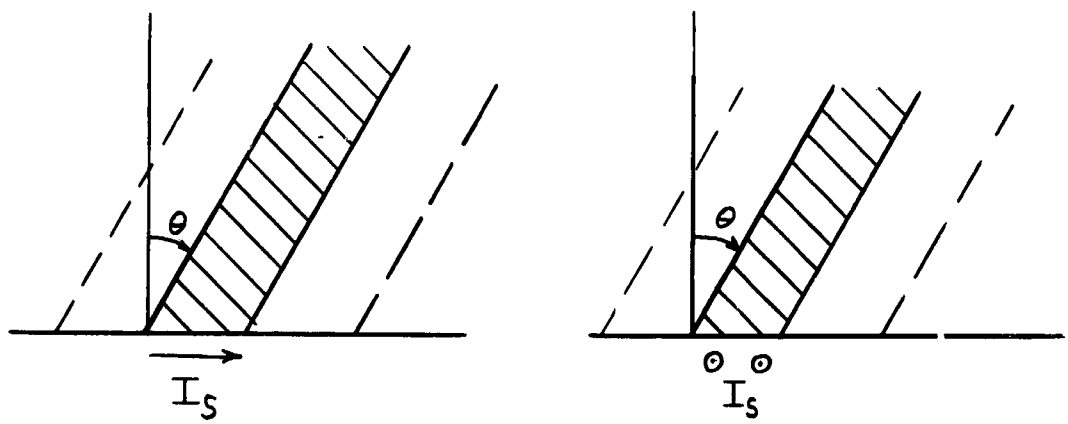

(a) E-plane scan (b) H-plane scan

Fig. 18 Unit Cell in Infinite Array

short slots or dipoles.

By the equivalence principle [31] most array source elements can be described by the appropriate combination of surface currents or current filaments (magnetic/electric). For an E-plane scan the effective electric current contributing to the far-field (E_θ) is

$$I_{eff} = I_s \cos \theta \tag{4-1}$$

implying

$$R_{eff} = \frac{R_o}{\cos \theta} \tag{4-2}$$

where R_o = broadside cell impedance.

Similarly, for the H-plane scan

$$I_{eff} = \frac{I_s}{\cos \theta} \tag{4-3}$$

implying

$$R_{eff} = R_o \cos \theta \, . \tag{4-4}$$

If mutual coupling is ignored, the above approach shows that the approximate impedance or admittance variation of the array with scan angle, θ, takes one of forms given in the following table:

E/H-plane	H/E-plane
cos	$\frac{1}{\cos \theta}$

The effective impedance variations, as well as the resultant reflection coefficients for these cases, are shown plotted in Fig. 19 below.

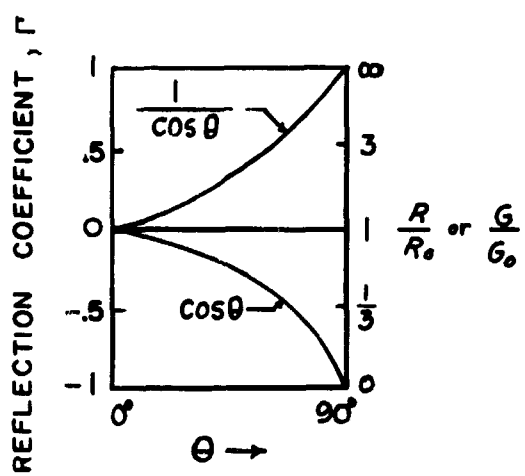

Fig. 19 Approximate Impedance and Reflection Coefficient Variation with Scan Angle

B. Planar Arrays of Short Dipoles

For an infinite array of short dipoles and in the absence of a ground plane, the active impedance for an arbitrary scan position (θ, ϕ) can be shown to be [7]

$$Z_a = \frac{N}{2\, d_x\, d_y} \sqrt{\frac{\mu}{\epsilon}} \left(\frac{1 - \sin^2\theta\cos^2\phi}{\cos\theta}\right) + i\, \frac{N\, X}{d_x\, d_y} \tag{4-5}$$

where

$$X = \frac{1}{2} \sqrt{\frac{\mu}{\epsilon}} \sum_m{}' \sum_n{}' \frac{\left[\sin\theta\cos\phi + \frac{m\lambda}{d_x}\right]^2 - 1}{\left[\left(\sin\theta\cos\phi + \frac{m\lambda}{d_x}\right)^2 + \left(\sin\theta\sin\phi + \frac{n\lambda}{d_y}\right)^2 - 1\right]^{1/2}} \tag{4-6}$$

N = constant dependent on type of element and geometry

$\sum'$ excludes the propagating modes.

If this array is placed a height, h, above a conducting ground plane, the active impedance becomes [7]

$$Z_a = R_a + i\, X_a$$

where

$$R_a = \frac{N}{d_x\, d_y} \overbrace{\sqrt{\frac{\mu}{\epsilon}} \left[\frac{1 - \sin^2\theta\cos^2\phi}{\cos\theta}\right]}^{Z_o} \sin^2(kh\cos\theta)$$

$$\triangleq \left[\frac{N}{d_x\, d_y}\right] Z_o \sin^2(hk\cos\theta)$$

$$X_a = \frac{N}{d_y\, d_x} \left[X + \frac{Z_o}{2} \sin(2\,kh\cos\theta)\right] .$$

The resistive components of impedance for the case without the ground plane and for the array positioned $\lambda/4$ above a ground plane are compared in Fig. 20 below.

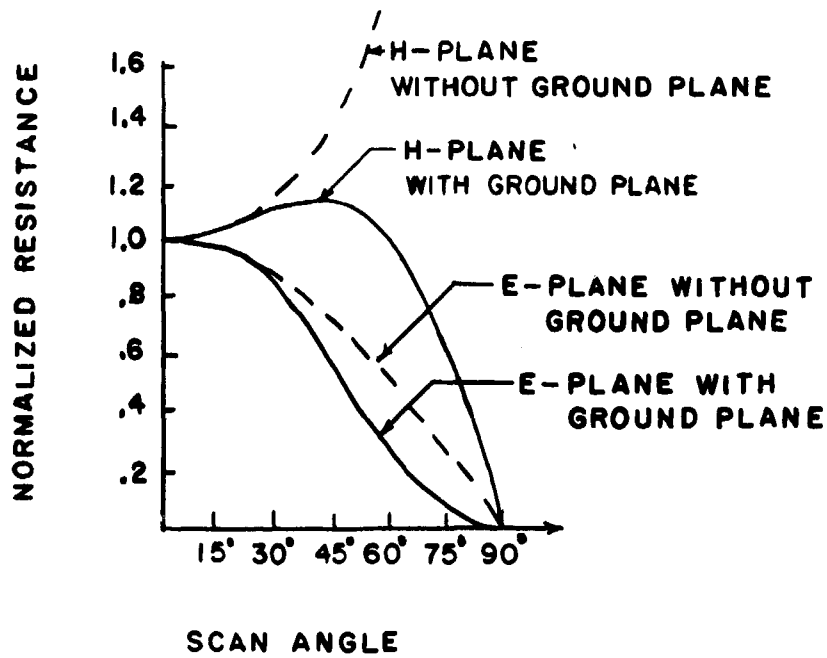

Fig. 20 Resistance versus Scan Angle

Note that for H-plane scan the ground plane reduces the VSWR to less than 1.2 for $\theta \leq 65°$.

C. Ground Plane, Grating Lobe, and Element Spacing Effects in Half-wave Dipole Arrays

In this section the behavior of some infinite or very large planar arrays of $\lambda/2$ dipoles are graphically presented.

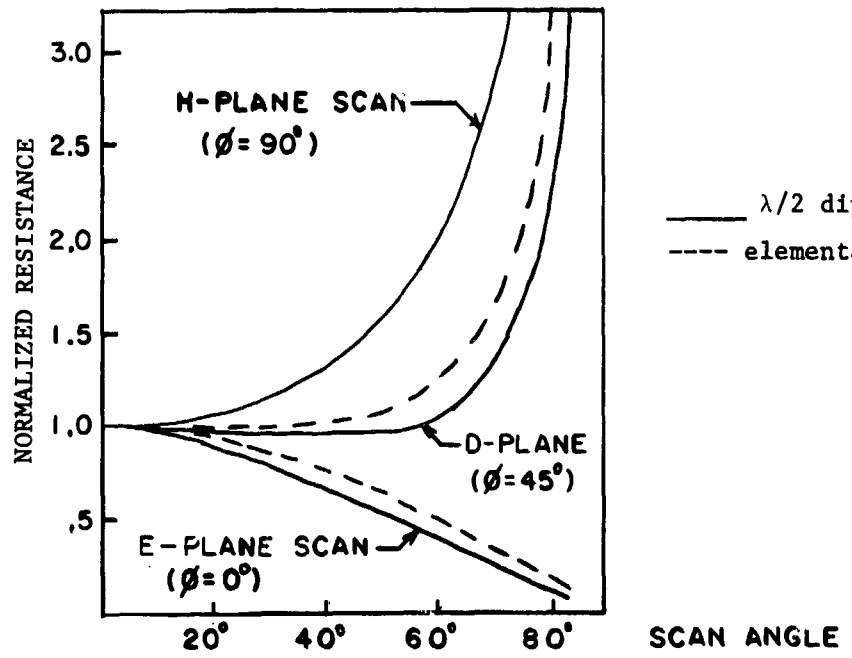

(a) Without ground plane

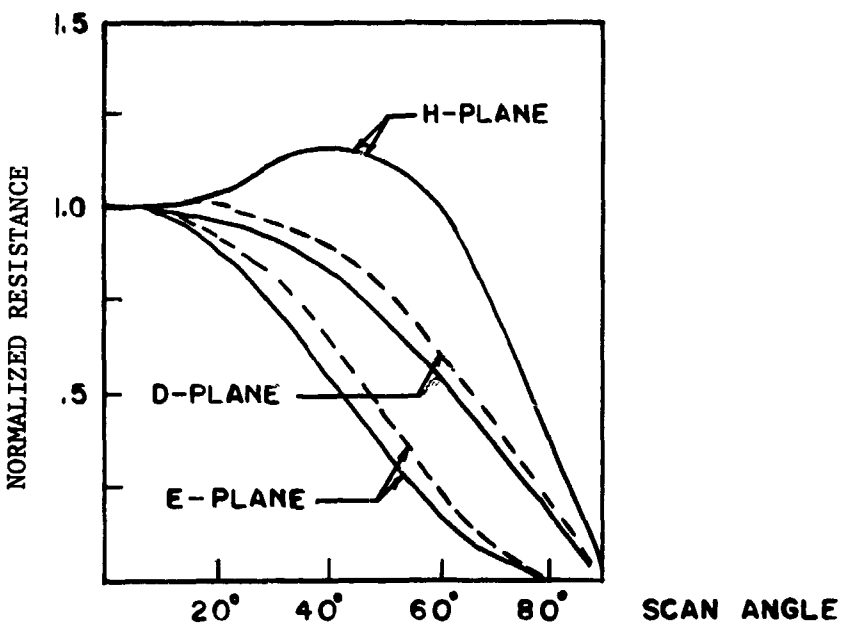

(b) With ground plane

Fig. 21 Effect of Ground Plane on Dipole Array Resistance

In Fig. 21 it is observed that with the ground plane:(1) D-and H-plane resistances go to 0 instead of infinity as $\theta \rightarrow 90°$ and (2) H-plane resistance is fairly constant out to scans of 60°.

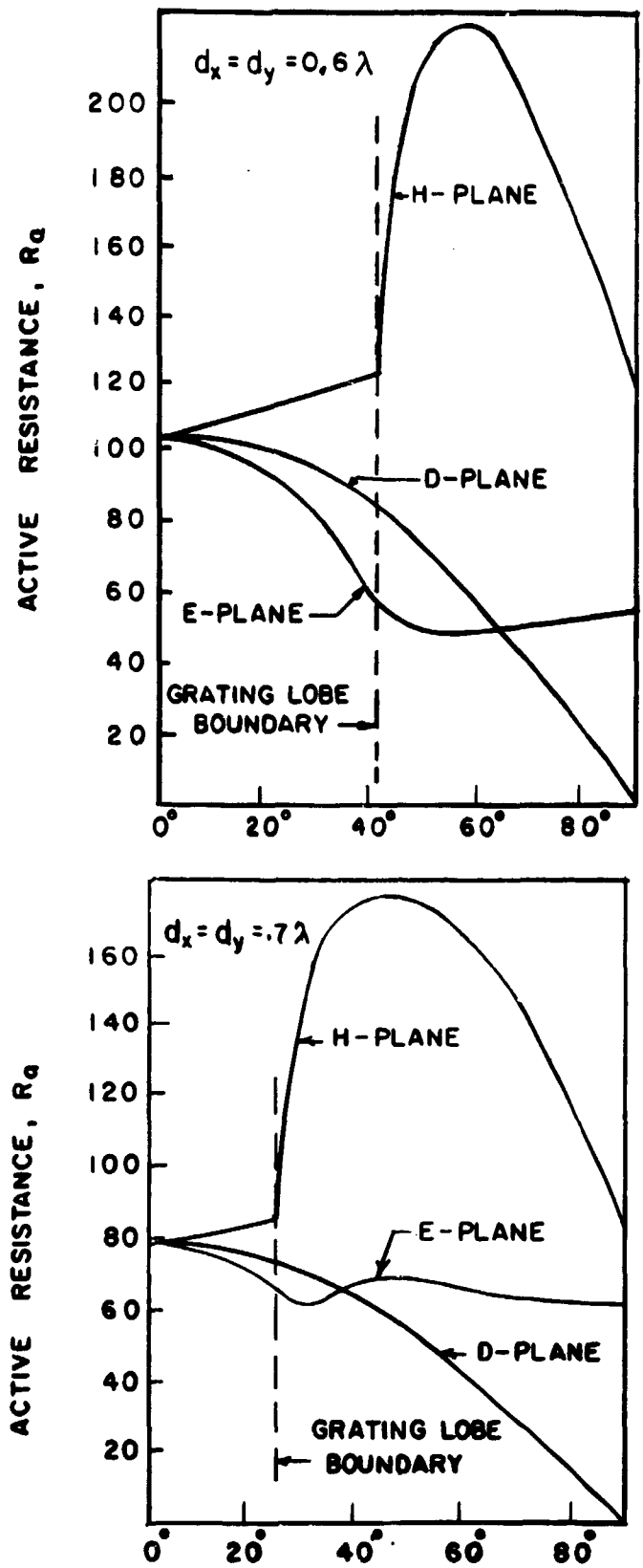

Fig. 22 Spacing and Grating Lobe Effects on Impedance ($\lambda/2$ dipoles, $\lambda/4$ above a ground plane) [8]

Comments on Fig. 22:

(1) The introduction of the grating lobe into visible space greatly perturbs impedance and efficiency.

(2) The broadside resistance was reduced from 105 to 80 ohms as the element spacing was changed from 0.6λ to 0.7λ.

(3) A 65x149 array was calculated to almost exactly fit the above curves for infinite arrays.

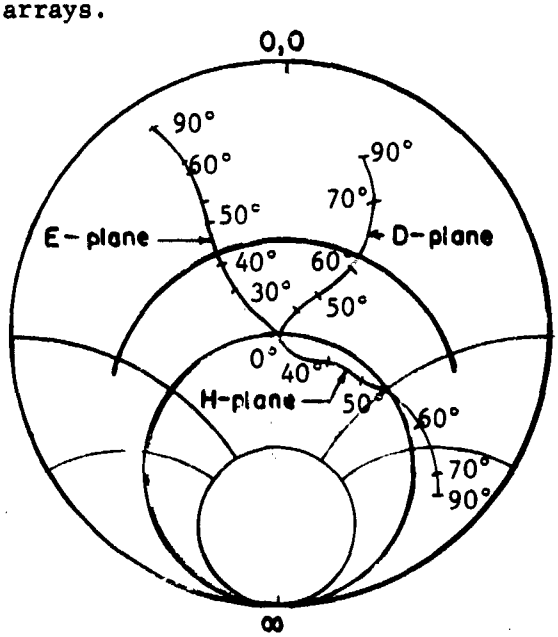

Fig. 23 Smith Chart Locus of Driving Impedance Variations with Scan Angle (λ/2 dipoles, $d_x = d_y = \lambda/2$) [9]

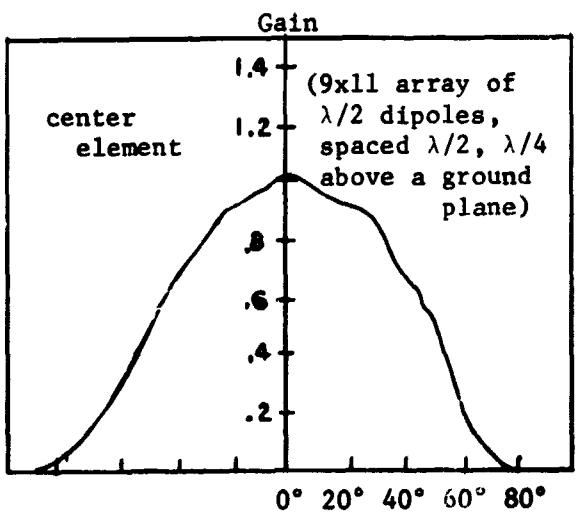

Fig. 24 E-Plane Gain vs Scan Angle [9]

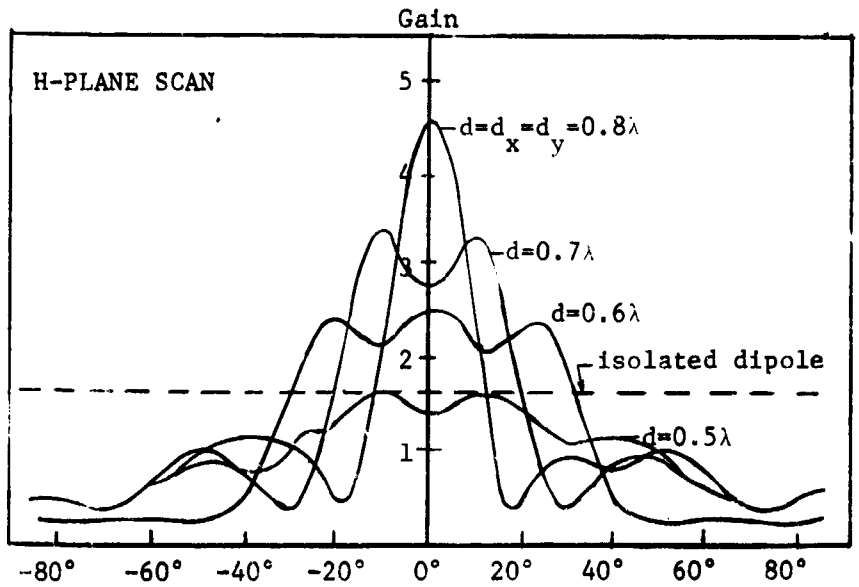

Fig. 25 Effect of Element Spacing on Gain vs Scan Angle (7x9 array of λ/2 dipoles) [10]

D. Calculations of Active Impedance and Efficiency for an Infinite Linear Array of Dipoles

As an example of the procedure involved in a theoretical analysis of impedance and efficiency effects, it is useful to consider Wasylkiwskyj and Kahn's [11] treatment of an infinite, linear array of elementary dipoles. In contrast to the earlier section on element efficiency, the influences of physical elements on the system and their contributions to mutual coupling will be included in this solution. Among the results obtained are the observations (1) that the impedance variation with scan angle is dependent on the orientation of the dipole elements with respect to the array axis and (2) that there exists an alignment where the impedance is a constant, independent of scan angle.

The solution is obtained by using the "free excitation" method [12] which models the drive to each array antenna element with an appropriately phased generator source having an impedance, Z_g (Fig. 26). The system is then analyzed in terms of the scattering or coupling coefficients at the interface to the radiating elements. A distinctive property of such a feed system is that it has constant incident or "available" power.

As a review, the basic equations and definitions used for scattering are noted. The scattering matrix equation is

$$[b] = [S][a], \tag{4-7}$$

and the equation governing a single port for a linear array is

$$b_n = \lim_{N\to\infty} \sum_{-N}^{N} S_{nm}\, a_m$$

$$= \lim_{N\to\infty} \sum_{-N}^{N} C_{nm}\, a_m \qquad (4\text{-}8)$$

where

a_m = incident wave from the m^{th} port = V^+/Z_g

b_n = reflected wave at the n^{th} port = V^-/Z_g

$S_{nm} = C_{nm} = \left.\frac{bn}{am}\right|_{aj = 0,\ j \neq m}$ = scattering or coupling coefficient

The quantity S_{nm} traditionally has been used to denote a scattering coefficient. In this treatment it will be used interchangeably with the term "coupling coefficient" denoted C_{nm} which is often adopted by those working in array theory. Unless stated otherwise, the symbol C_{nm} will be used throughout the remainder of this report. In terms of the total voltage and current

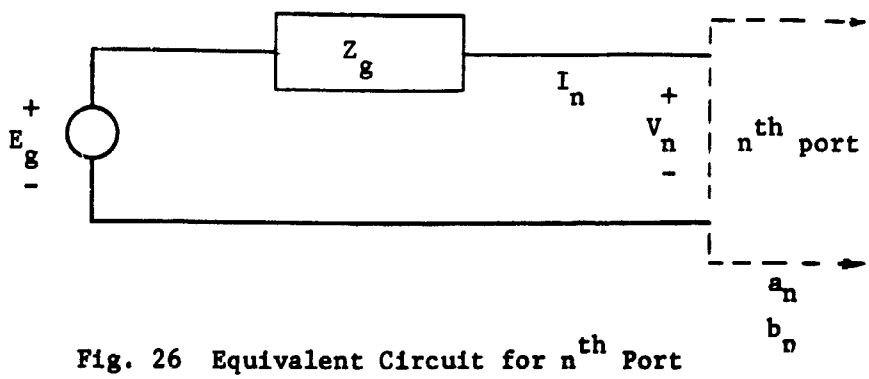

Fig. 26 Equivalent Circuit for n^{th} Port

at the n^{th} port it can be shown that

$$V_n + Z_g I_n = 2\sqrt{R_g}\, a_n \tag{4-9}$$

$$V_n - Z_g^* I_n = 2\sqrt{R_g}\, b_n \tag{4-10}$$

where $Z_g = R_g + i X_g$ = generator impedance. It is also a consequence of the definition of scattering coefficients that

$$|S_{nm}|^2 = \frac{\text{power to n}}{\text{power available at n due to m with all other ports passively terminated in } Z_g}$$

which again makes obvious the origin of the term, coupling coefficient. Note that Debski and Hannan [13] showed that it is possible to measure these parameters and use the results as the basis for calculations of active array performance. Their scheme involves a passive array measurement where one element is excited, the rest are terminated in their matched generator impedances, and the wave transfers to various elements are measured to determine respective coupling coefficients.

For the infinite linear array of dipoles shown in Fig. 27 (all lie in the xy-plane and are oriented at an angle γ_o with respect to the array axis),

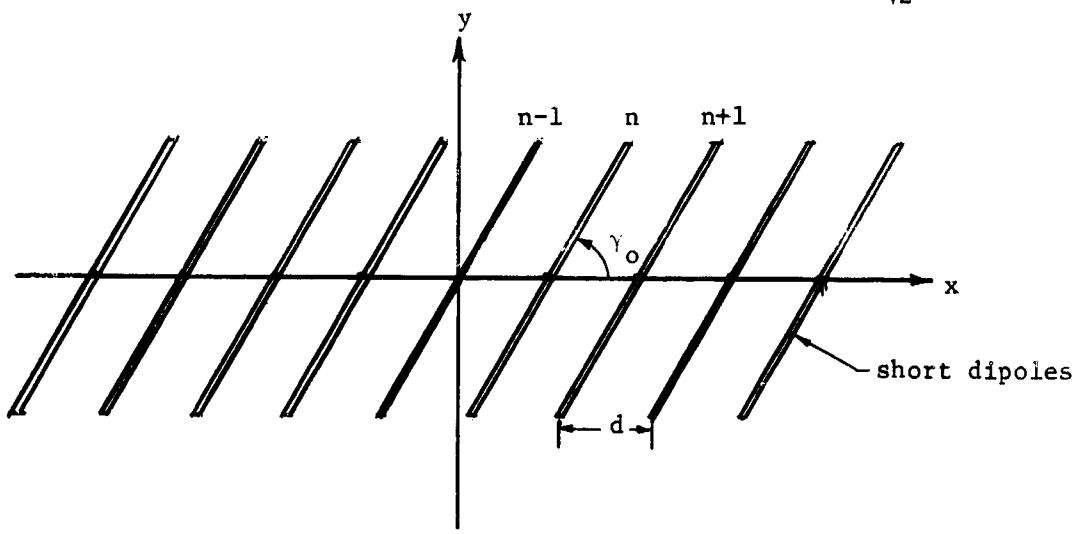

Fig. 27 Infinite Linear Array of Short Dipoles

the voltage at the n^{th} port is given by an infinite difference equation

$$V_n = \lim_{N\to\infty} \sum_{-N}^{N} z_k \, I_{n+k} \qquad (4\text{-}11)$$

$$z_k = \frac{V_n}{I_{n+k}}$$
all other I's = 0 . (4-12)

Desiring to further correlate the impedance and coupling relations at the n^{th} port, the following approach is taken. From (4-9) for $a_m = 0$ it follows that

$$V_m = -Z_g \, I_m \Big|_{a_m = 0} \qquad (4\text{-}13)$$

Substituting (4-13) into (4-10) yields

$$b_m \Big|_{a_m = 0} = \frac{1}{2\sqrt{R_g}} \left[-Z_g - Z_g^* \right] I_m = -\sqrt{R_g}\ I_m \tag{4-14}$$

Therefore

$$C_{nm} = \frac{b_m}{a_n}\Big|_{\substack{a_j = 0 \\ j \neq n}} = -\sqrt{\frac{R_g}{a_n}}\ I_m \quad \text{for } n \neq m \tag{4-15}$$

and similarly

$$C_{nn} = 1 - \sqrt{R_g}\ \frac{I_m}{a_n} \quad \text{for } n = m. \tag{4-16}$$

By substituting the expansion (4-11) into (4-9), (4-9) can be written

$$2\sqrt{R_g}\ a_m = \lim_{N \to \infty} \sum_{-N}^{N} z_k\ I_{m+k} + I_m\ Z_g \tag{4-17}$$

Now an excitation is applied at m which is adjusted to cause a net wave of unity to be incident at n. Equation (4-17) becomes

$$2\sqrt{R_g}\ \hat{a}_{mn} = 2\sqrt{R_g}\ \delta_{nm} = \sum z_k\ \hat{I}_{n+k,m} + Z_g\ \hat{I}_{n,m} \tag{4-18}$$

where $\hat{a}_{nm} = \delta_{nm}$ = unit incident wave at n due to the excitation at m with all other ports passively terminated in Z_g

$\hat{I}_{p,m}$ = current at p due to the above excitation at m.

If $\hat{I}_{n,m}$ are constrained such that $\sum_{-\infty}^{\infty} \left|\hat{I}_{n,m}\right|^2 < \infty$ and if

$$\delta_{mn} = \frac{1}{2\pi} \int_{-\pi}^{\pi} e^{-i(m-n)\xi} \, d\xi = \text{Kronecker delta,} \tag{4-19}$$

then $\hat{I}_{n,m}$ can be made the n^{th} term coefficient in a Fourier series expansion of a function $F(\xi)$

$$\hat{I}_{n,m} = \frac{1}{2\pi} \int_{-\pi}^{\pi} F(\xi) \, e^{-i(n-m)\xi} \, d\xi \tag{4-20}$$

Using (4-19) and (4-20) in (4-18) yields

$$2\sqrt{R_g} \; \frac{1}{2\pi} \int_{-\pi}^{\pi} e^{-i(n-m)\xi} \, d\xi = \sum_k z_k \frac{1}{2\pi} \int_{-\pi}^{\pi} F(\xi) e^{-i(n+k-m)\xi} \, d\xi$$

$$+ Z_g \frac{1}{2\pi} \int_{-\pi}^{\pi} F(\xi) \, e^{-i(n-m)\xi} \, d\xi \tag{4-21}$$

Then equating integrands in (4-21) and solving for $F(\xi)$ gives

$$F(\xi) = \frac{2\sqrt{R_g}}{Z_g + \sum z_k e^{-ik\xi}} = \frac{2\sqrt{R_g}}{Z_g + Z(\xi)} \tag{4-22}$$

where $Z(\xi)$ is defined as

$$Z(\xi) = \lim_{N\to\infty} \sum_{-N}^{N} z_k e^{-ik\xi} \; . \tag{4-23}$$

The current $\hat{I}_{nm}$ is thus

$$\hat{I}_{nm} = \frac{1}{2\pi} \int_{-\pi}^{\pi} \frac{2\sqrt{R_g}}{Z_g + Z(\xi)} e^{-i\xi(n-m)} \, d\xi \quad , \tag{4-24}$$

and by superposition the total current at n is

$$I_n = \sum_{m=-\infty}^{\infty} \hat{I}_{n,m} \; a_m = \frac{1}{2\pi} \int_{-\pi}^{\pi} \frac{2\sqrt{R_g}}{Z_g + Z(\xi)} \left[\sum_{-\infty}^{\infty} a_m e^{im\xi} \right] e^{-in\xi} \, d\xi \tag{4-25}$$

Consequently the scattering matrix elements can be expressed

$$C_{nm} = \delta_{mn} - \frac{R_g}{\pi} \int_{-\pi}^{\pi} \frac{e^{-i\xi(n-m)}}{Z_g + Z(\xi)} \, d\xi \tag{4-26}$$

or using (4-19) for δ_{nm} and manipulating (4-26) the coupling coefficient expression can be rearranged to give (*denotes complex conjugate)

$$C_{nm} = \frac{1}{2} \int_{-\pi}^{\pi} \frac{Z(\xi) - Z_g^*}{Z(\xi) + Z_g} e^{-i\xi(n-m)} \, d\xi \; . \tag{4-27}$$

It is now noted that

$$Z(\alpha) = \lim_{N \to \infty} \sum_{-N}^{N} z_p e^{-ip\alpha}$$

is identical to the active impedance of an infinite array excited by equal amplitudes and a linear phase taper, α. This is true because for $a_m = e^{-im\alpha}$ the sum in the integrand of (4-25) equals $2\pi\delta(\xi-\alpha)$ where δ is the Dirac delta function, and hence integration of (4-25) produces

$$I_n(\alpha) = \frac{2\sqrt{R_g}}{Z_g + Z(\alpha)}\ e^{-in\alpha}$$

$$\alpha = \text{phase taper} = kd \sin\theta$$

which can be written

$$Z_g + Z(\alpha)\ I_n(\alpha) = 2\sqrt{R_g}\ e^{-in\alpha} \quad . \tag{4-28}$$

Looking at (4-9) with $a_n = e^{-in\alpha}$

$$2\sqrt{R_g}\ a_n = 2\sqrt{R_g}\ e^{-in\alpha} = V_n + I_n Z_g$$

and comparing with (4-28), it is immediately apparent that

$$V_n = Z(\alpha)\ I_n(\alpha)$$

or

$$Z(\alpha) = \frac{V_n}{I_n} = \text{active input impedance of the } n^{th} \text{ port.} \tag{4-29}$$

Since $Z(\alpha)$ is the load impedance seen by the generator at the n^{th} element, the reflection coefficient is

$$\Gamma(\alpha) = \frac{Z(\alpha) - Z_g^*}{Z(\alpha) + Z_g} \quad . \tag{4-30}$$

But Eq. 4-27 then implies that C_{mn} are the Fourier series coefficients in an expansion for $\Gamma(\alpha)$. Hence, it is seen that

$$\Gamma(\alpha) = \sum_{m=-\infty}^{\infty} C_{nm}\, e^{i(n-m)\alpha} = \frac{Z(\alpha) - Z_g^*}{Z(\alpha) + Z_g} \quad , \tag{4-31}$$

and

$$C_{nm} = \frac{1}{2\pi} \int_{-\pi}^{\pi} \Gamma(\alpha)\, e^{-i(n-m)\alpha}\, d\alpha$$

$$= \frac{1}{2\pi} \int_{-\pi}^{\pi} \frac{Z(\alpha) - Z_g^*}{Z(\alpha) + Z_g}\, e^{-i(n-m)\alpha}\, d\alpha \quad . \tag{4-32}$$

From Eqs. 4-30, 4-31, and 4-32 it is thus possible to determine active element impedance variations with scan knowing the reflection coefficient behavior and to relate coupling coefficients to the reflection coefficient. Although these results were obtained for a one-dimensional array, the same procedures can be employed to extend them to multi-dimensional arrays.

Recalling the definition of element efficiency given on page 16

$$\eta = 1 - \frac{\text{power reflected}}{\text{power available}} = \frac{\text{power radiated}}{\text{power available}} \tag{4-33}$$

and using the above formulations, it follows from Parseval's theorem that

$$\eta = 1 - \sum_{m} |C_{nm}|^2 = 1 - \frac{1}{2\pi} \int_{-\pi}^{\pi} |\Gamma(\alpha)|^2 \, d\alpha$$

$$= 1 - \frac{1}{2\pi} \int_{-\pi}^{\pi} \left| \frac{Z(\alpha) - Z_g^*}{Z(\alpha) + Z_g} \right|^2 d\alpha \qquad (4\text{-}34)$$

Taking the first term on the right hand side into the integral and doing the required algebra yields

$$\eta = \frac{1}{2\pi} \int_{-\pi}^{\pi} \frac{|Z+Z_g|^2 - |Z-Z_g^*|^2}{|Z+Z_g|^2} \, d\alpha = \frac{2R_g}{\pi} \int_{-\pi}^{\pi} \frac{\text{Real}[Z(\alpha)]}{|Z(\alpha)+Z_g|^2} \, d\alpha \qquad (4\text{-}35)$$

From (4-34) a linear array having a phase taper $\alpha_s = kd \sin\theta_s$ is seen to be impedance matched at the scan angle, θ_s, if

$$Z_g^* = Z(\alpha_s) \; . \qquad (4\text{-}36)$$

The invisible-visible region constraints give

$$\text{Real}[Z(\alpha)] \geq 0 \text{ and } |\Gamma(\alpha)| \leq 1 \text{ for } |\alpha| < kd < \pi \qquad \text{(a)}$$

$$\text{Real}[Z(\alpha)] = 0 \text{ and } |\Gamma(\alpha)| = 1 \text{ for } kd < |\alpha| \; . \qquad \text{(b)} \qquad (4\text{-}37)$$

For the conditions in (4-37a) real power is radiated, and for the conditions of (4-37b), $Z(\alpha)$ is purely reactive and there is no time average power.

Since the visible region accounts for the radiated power, Eq. 4-35 can be written

$$\eta = \frac{2R_g}{\pi} \int_{-kd}^{kd} \frac{\text{Real}[Z]}{|Z_g+Z|^2}\, d\alpha \quad \text{for } 0 \leq kd \leq \pi \,. \tag{4-38}$$

Again using Hannan's definition of an "ideal" element as one which is matched for all angles of scan in the visible region, i.e. $Z_g^* = Z(\alpha)$ for all $|\alpha| \leq kd$, the <u>maximum</u> or <u>ideal efficiency</u> for an infinite linear array is found to be

$$\eta_{max} = \frac{2R_g}{\pi} \int_{-kd}^{kd} \frac{R_g}{(2R_g)^2}\, d\alpha = \begin{cases} \frac{kd}{\pi}, & kd < \pi \\ 1.0, & kd \geq \pi \,. \end{cases} \tag{4-39}$$

Wasylkiwskyj and Kahn [14] calculated impedance and efficiency for an infinite linear array of elementary dipoles. The impedance terms, z_ν, for elementary dipoles are given by

$$z_\nu = \frac{3}{2}\left[h_o^{(2)}[|\nu|kd] - \frac{h_1^{(2)}[|\nu|kd]}{|\nu|\,kd} \right] \sin^2\gamma_o +$$

$$\frac{3h_1^{(2)}[|\nu|kd]}{|\nu|kd} \cos^2\gamma_o \,, \quad \nu \neq 0$$

$$z_\nu = 1.0 \,, \quad \nu = 0$$

where γ_o = angle between each dipole and the array axis, $h_o^{(2)}$ and $h_1^{(2)}$ are spherical Hankel functions. They substituted (4-40) into (4-23) and summed it to get an expression for $Z(\alpha) = R_a + i X_a$. In closed form their result for $R_a = Re[Z]$ is

$$R_a = \frac{3\pi}{2kd} \left[\left(1 - \frac{\alpha^2}{k^2 d^2}\right)\left(\cos^2\gamma_o - \frac{1}{2}\sin^2\gamma_o\right) + \sin^2\gamma_o \right] , \quad |\alpha| < kd < \pi$$

$$= 0 , \quad kd < |\alpha| \qquad (4\text{-}41)$$

For an element spacing of $\lambda/4$, Eq. 4-41 is plotted for several dipole orientations, γ_o, in Fig. 28 below.

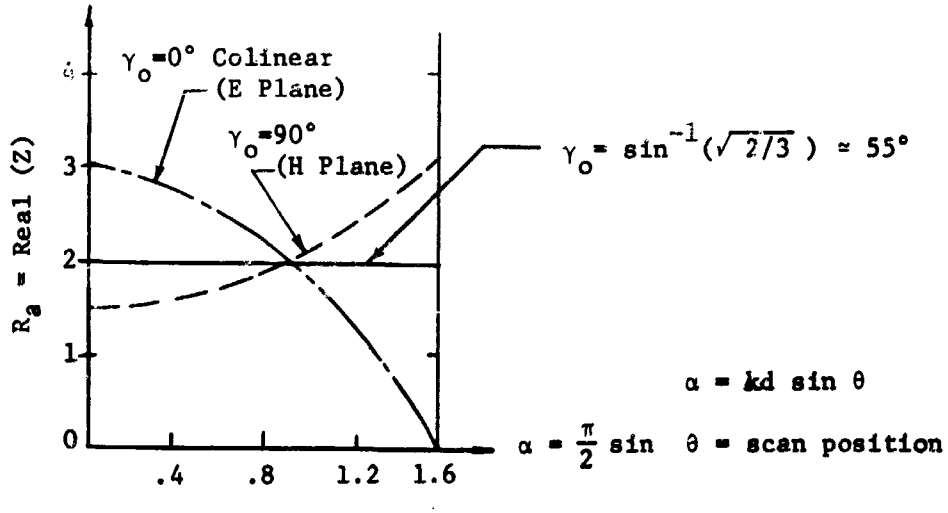

Fig. 28 Active Resistance vs Scan Angle for an Infinite Linear Array of Elementary Dipoles (kd = π/2)

From (4-41) and Fig. 28 it is seen that an important special case occurs when $\sin^2\gamma_o = 2/3$. This yields

$$\text{Re}(Z) = \frac{\pi}{kd} \quad , \qquad |\alpha| < kd < \pi$$

$$= 0 \quad , \quad kd < |\alpha|$$

which is <u>constant and independent of scan angle</u>. The element efficiency for the optimum alignment [$\sin(\gamma_o) = \sqrt{2/3}$] has been calculated and is shown in Fig. 29.

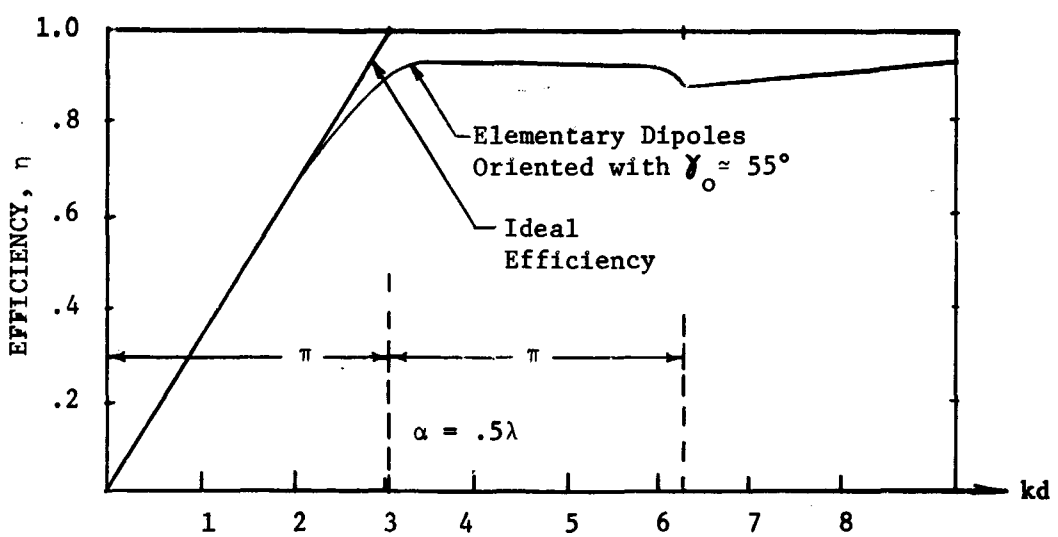

Fig. 29 Effect of Element Spacing on Efficiency (sin $\gamma_o = \sqrt{2/3}$)

Note that the above analysis suggests a theoretical justification for the common technique of mounting crossed slots or crossed dipoles in a planar array at 45° with respect to the array axes in that impedance variations with scan angle tend to be reduced.

E. Coupling Wave Effects Producing Mismatch Prior to the Appearance of Grating Lobes [15]

Surface waves (or as Knittel, Oliner, et al. [16, 39] have pointed out, surface-wave-like fields, or sometimes leaky waves) along an array face can destructively interfere with the generator phased elements with the net result that large reflections occur at the effective array surface. Under such conditions of large reflection, the efficiency of the array becomes intolerably low and the drive networks become badly matched. Thus, if coupling waves initiated along an array produce the first destructive interference seen by the beam as it is scanned from broadside, the coupling waves, not grating lobes, will determine the scan limits for that array. This discussion presents an intuitive explanation of the phenomenon in terms of coupling or "surface" waves, and the results can be applied to any array, not just ones covered with thick dielectric sheets where true surface waves cause the effect. The development to follow depends on the observation that if coupling effects somehow propagate along the surface of an array with a coupling velocity less than the speed of light (slow wave), coupling mismatches will occur and degrade efficiency at smaller scan angles than those at which grating lobes appear. In practice many arrays exhibit slow wave coupling velocities, and this is evidenced by mismatches at angles prior to those predicted by grating lobes [19].

For this analysis a planar array with an equilateral triangular grid such as shown in Fig. 30 is considered. As is well known, an equilateral triangular grid (hexagonal cell) reduces the number of elements required by 13.4% [2], and because of its consequent widespread usage, it will be investigated here. In such a lattice a cardinal plane

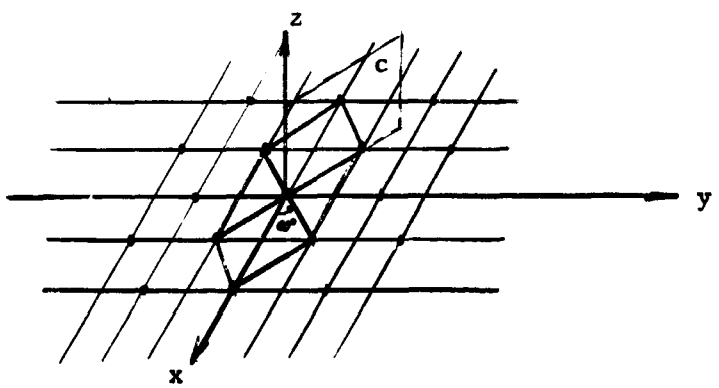

Fig. 30 Cardinal and Intercardinal Planes

is defined as one containing the z axis and any one of the six closest elements (i.e., $\phi = 0°, 60°, 120°, 180°, 240°, 300°$), and an intercardinal plane contains the z axis and one of the bisecting planes ($\phi = \pm 30°, \pm 90°, \pm 150°$). In the case of a planar array the active reflection coefficient at the center element (0, 0) with all others excited is given by

$$\Gamma = \sum_m \sum_n C_{mn} \frac{V_{mn}}{V_{00}} \qquad (4\text{-}42)$$

where

C_{mn} = mutual coupling coefficient between the $(0,0)^{th}$ and $(m,n)^{th}$ antenna elements

V_{mn} = drive voltage applied to the $(m,n)^{th}$ element

V_{00} = drive voltage applied to the $(0,0)^{th}$ element.

For a two-dimensional planar array having a uniform amplitude illumination, the beam is steered in the (θ_s,ϕ_s) direction by phasing the elements such that

$$\frac{V_{mn}}{V_{00}} = \exp[-im\psi_x - in\psi_y] \tag{4-43}$$

where

$$\psi_x = k\, d_x \sin\theta_s \cos\phi_s$$
$$\psi_y = k\, d_y \sin\theta_s \sin\phi_s \,.$$

The resulting far-field pattern factor is then given by

$$F(\theta,\phi) = \sum \sum \exp[imk\, d_x(\sin\theta\cos\phi - \sin\theta_s \cos\phi_s) + ink\, d_y(\sin\theta \sin\phi - \sin\theta_s \sin\phi_s)] \tag{4-44}$$

For this phasing Eq. 4-42 is recognized as a Fourier series

$$\Gamma(\psi_x,\psi_y) = \sum_m \sum_n C_{mn}\, e^{-im\psi_x - in\psi_y} \,, \tag{4-45}$$

and hence the scattering or mutual coupling coefficients can be found from

$$C_{mn} = \frac{1}{(2\pi)^2} \int_{-\pi}^{\pi} \int_{-\pi}^{\pi} \Gamma(\psi_x,\psi_y)\, e^{im\psi_x + in\psi_y}\, d\psi_x\, d\psi_y \,. \tag{4-46}$$

In order to simplify the analysis the special case of scanning in the cardinal plane, $\phi_s = 0$, is considered. Here $\psi_y = 0$ and $\psi_x = k\, d_x \sin\theta$ reducing (4-45) to

$$\Gamma(\psi_x) = \sum \sum C_{mn}\, e^{-im\psi_x} = \sum_m A_m\, e^{i\phi_m - im\psi_x} \qquad (4\text{-}47)$$

where

$$A_m\, e^{i\phi_m} = \sum_n C_{mn} \quad .$$

Each element is the source of an electromagnetic wave which propagates out from it. Into free space the wave propagates at the velocity of light, however, along the array face it is possible that the array elements and the surface interact to create a coupling wave which travels parallel to the surface at an effective velocity other than the speed of light. Since the array is nearly infinite, it follows that the coupling velocity, and hence the phase shift, should be symmetric about the reference element along a line through it. Thus, for cardinal plane scan, the expected phase delay m elements from the reference is

$$\phi_m = a + |m|\bar{\phi} \qquad (4\text{-}48)$$

where

$$\bar{\phi} = \text{incremental phase delay in coupling}$$

$$= k_c\, d_x = \omega\, d_x / v_c = 2\pi d_x / \lambda_c \quad .$$

The above is expressed in terms of a real or fictitious coupling wave that travels outward from the 0^{th} column with a phase velocity, v_c.

Under these circumstances the reflection coefficient becomes

$$\Gamma(\psi_x) = \sum C_{On} + e^{ia} \sum_{1}^{\infty} A_m e^{-im(\psi_x - \bar{\phi})} + A_m e^{+im(\psi_x + \bar{\phi})} , \qquad (4\text{-}49)$$

and large coupling mismatches occur when the coupling contributions add in-phase to maximize Γ. From Eq. 4-49 it is seen that this takes place when

$$\psi_x = \pm \bar{\phi} + 2\pi p = k\, d_x \sin\theta_c = \pm \frac{2\pi d_x}{\lambda_c} + 2\pi p . \qquad (4\text{-}50)$$

Solving the above for the critical scan angle due to coupling gives

$$\sin\theta_c = \frac{p\lambda_o}{d_x} \pm \frac{\lambda_o}{\lambda_c} = p\,\frac{\lambda_o}{d_x} \pm \frac{c}{v_c} \qquad (4\text{-}51)$$

c = speed of light

Mismatches are gnerated when θ_c lies in real space, i.e. $|\sin\theta_c| \leq 1$. Since $p = 1$ commonly designates the threshold of the destructive interference in real space, the form of Eq. 4-51 normally used for calculations is

$$|\sin\theta_{gl}| = \frac{\lambda_o}{d_x} - \frac{c}{v_c} . \qquad (4\text{-}52)$$

From Chapter II the normally predicted grating lobe condition for this cardinal plane ($\phi_s = 0$) is given by

$$|\sin\theta_{gl}| = \frac{\lambda_o}{d_x} - 1 . \qquad (4\text{-}53)$$

Comparing Eqs. 4-52 and 4-53 it is noted for slow wave mutual coupling (as is often the case) where $v_c < c$ that $\theta_c < \theta_{gl}$, and hence mismatch due to mutual coupling is observed at scan angles prior to those predicted by pure grating lobe assumptions. Note that there have been many instances where experimental measurements have recorded this effect. Linearily polarized coaxial horns, circularily polarized coaxial horns, and linearily polarized rectangular horn arrays have all been characterized by coupling velocities less than the speed of light [18, 19, 20].

Using only the unmodified grating lobe condition of (4-53), the maximum element spacings to eliminate grating lobes for scans out to $\pm \theta_m$ are

$$d_x = \frac{\lambda_o}{1 + |\sin\theta_m|} \qquad (4\text{-}54)$$

and

$$d_y = \sqrt{3}\, d_x \quad \text{(hexagonal cell)}.$$

From Eq. 4-52 it is obvious that this choice can result in serious impedance mismatches, radiation loss, and polarization distortion whenever the element coupling phase velocity is less than the speed of light, as is frequently the case. The degradations are caused by the in-phase accumulation of coupling contributions, and in such instances the coupling accumlation determines the usuable scan limits for efficient operation without compensation. Actually this is just an alternate way of looking at the problem of impedance variations and mismatch with scan angle (caused by and commonly analyzed by mutual coupling considerations). Its advantage is that it lumps coupling effects in a propagation velocity,

v_c, which can be experimentally measured [15] or usefully employed as a design safety factor.

Lechtreck [20] did extensive experimental work with a 65 element planar array of coaxial horn antennas (hexagonal interelement geometry with a rectangular periphery). He considered:

(1) Polarization (linear and circular)

(2) Radomes (with and without)

(3) Cardinal and IC scan planes

(4) Interelement spacing

with the following results:

1. Phase, $\bar{\phi}$, was linearily proportional to $|m|$ or the magnitude of distance from the column used as a reference.

2. Coupling velocities (v_c) of 90 to 92% of c (velocity of light) were measured for linear and circular polarization.

3. Large gain and power losses occurred at the scan angles predicted using the coupling velocity, v_c.

4. The presence and shape of radomes affected the coupling velocity.

5. Figure 31 below shows the variation in θ_{sc} (critical scan angle) with element spacing for the range of coupling velocities encountered. Note that decreasing d_x gives a wider useful scan.

6. For circuilar polarization, a large polarization distortion occurred near θ_{sc} (critical coupling scan angle).

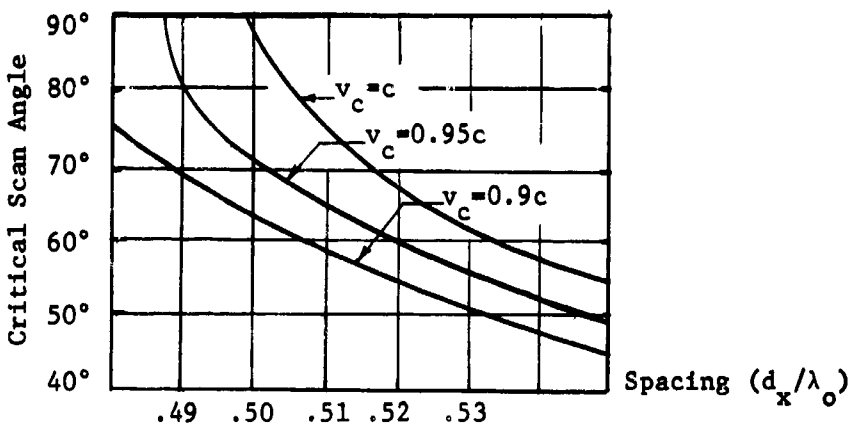

Fig. 31 Critical Scan Angle vs Spacing
(circularly polarized, 5x13 planar array)

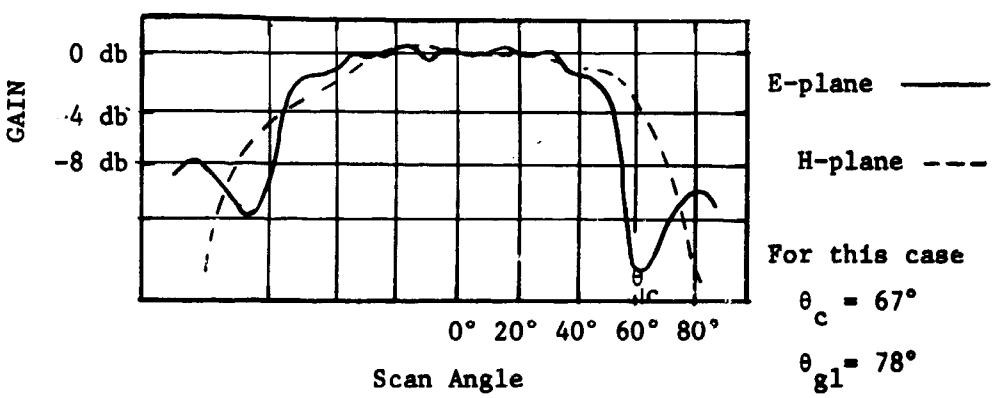

Fig. 32 Polarization Distortion
(5x13 planar array, $d_x = 0.506\lambda$)

F. Polarization Effects

Polarization will be treated in more detail in a future study [41] where special attention will be given to wide angle matching of circularly polarized arrays. Some qualitative aspects are summarized below. In the following list are some specific as well as general observations:

1. In arrays it is possible for linearly polarized elements to produce elliptical polarizations varying all the way to circular at certain scan angles. Similarly, circularly polarized source elements can display linear polarizations when used in an array. Often these effects are most pronounced near grating lobes. Fortunately, polarization degeneration is not a necessary occurrence for elements in an array environment, and in many instances the polarization characteristics of an array are better than those of an isolated antenna element.

2. Polarization deteriorization is strongly a function of the array geometry and the type of radiating element. For example polarization loss is more noticeable for dipoles in echelon than for a rectangular grid of dipoles.

3. For evaluating polarization effects it is usually easiest to measure or compute the cross polarization field component as a function of scan angle.

4. Gain for a desired mode of polarization can be substantially reduced by energy transferred to unwanted polarizations.

5. Under proper conditions the polarization of an array of crossed dipoles was found to be more nearly circular over wide scan angles than was the pattern of a single element (axial ratio at $\theta_s = 57°$ improved from 2.1:. to 1.11:1 when the element was placed in a 7 x 7 rectangular array [10]).

6. Log periodic antennas generally do not work well in arrays.

7. Spirals, crossed dipoles, crossed slots, cavity-backed circular and square apertures, helices, and specially designed combinations such as the Wheeler element [42] are commonly used for circular polarization.

8. Spiral antennas are useful for circular polarization. They are broadband and their relative phases can be adjusted by rotation of the feeds.

9. Flush mounted antenna elements are preferred in many array designs. Since the feed structures for nonflush antennas protrude into the fields of adjacent array elements, the mutual coupling effects can be considerable and are difficult to predict. A shadowing phenomenon can occur which especially limits wide angle scans. Lastly, the aerodynamic advantages of flush mounted radiators are obvious.

10. For wide angle scans an ideal element would be one with a hemispherically isotropic pattern with the proper polarization. The beam width of an individual element in an array with all other elements terminated in matched impedances is a good measure of the maximum scan range for the active array.

11. Scott and Soo Hoo [43] have shown that a null-free antenna pattern includes all axial ratios. Thus it is impossible to achieve a null-free antenna pattern with a fixed polarization. By applying topological theorems Scott [44] showed that a circularly polarized antenna requires at least one null point in its far field pattern.

V. COMPENSATION TECHNIQUES

In this chapter some of the techniques for compensating an array for changes in element driving point impedance with scan angle will be considered. Again since impedance changes produce great losses in gain and efficiency at extreme scan angles, any lossless schemes for reducing effective impedance variations will also improve efficiency.

A. FOR PRELIMINARY DESIGN OR LAB STUDY MODELS

The components listed below are readily available and provide a means of isolating the array generators or loads from the effects of the impedance variations at the antenna elements. Generally these matching networks are lossy and hence are best applied to designs having no premium on radiated power or efficiency, such as might be the case with mock-up or experimental designs where simplicity and speed of implementation are important. Some of the off-the-shelf components used for such matching are given as follows:

1. Series pads to reduce VSWR
2. Terminated circulators
3. Isolators

All of the above give isolation between the feed network and the array elements thereby reducing standing waves and helping prevent oscillator pulling and parametric oscillations, however, most of them fail to cope with the basic efficiency problem of variation in realized gain with scan angle.

B. CORRECTIVE COMPENSATIONS

In arrays where radiated power and efficiency are important the problems of mutual coupling and impedance changes with scan angle must be considered. As an arbitrary rule of thumb it noted that for scans of less than $\pm$ 30° from broadside, mismatch effects are usually tolerable. However, depending on the array and grid geometry, efficiency losses due to impedance changes seriously affect array performance for scans beyond certain limits. For instance, planar arrays are typically used for scans up to $\pm$ 60° from broadside, and in many cases compensation techniques can be very effective in achieving efficient scans over that range. For scans much greater than $\pm$ 60° it is probably best to go to three-dimensional array geometries to maintain reasonable efficiencies. This work will concentrate on linear and planar arrays since these geometries are frequently used as building blocks for more general configurations. Knittel [21] and Kmetzo [22], for instance, have considered hemispheric scan coverage using planar arrays arranged in a pyramidal fashion.

Basically there are two general approaches to the task of lossless scan matching, namely,

1. Modification of the array environment with fences, baffles, dielectric cover sheets, or dielectric plugs [23,24,25],
2. Employment of tunable active or passive matching networks and/or interconnecting circuitry between array elements [26,27,28].

Of the following methods the most applicable are probably variations of the Hannan connecting circuit technique [26] and the Magill and Wheeler sheet matching [24]. Because of the importance of these methods much of this work is done to supplement them and present their limitations so that

hopefully most of the information needed for actual design is readily available. The matching dielectric sheet is essentially a trial and error procedure where the primary limitation is the necessity of avoiding deleterious coupling wave effects. Hannan's connecting circuit method is probably the most powerful, but it has a greater initial cost and requires either a fairly reliable experimental measurement of impedance and coupling variations with scan angle or a detailed theoretical study giving the same information. The complexity of the corrective compensation scheme used depends on the degree of compensation desired. First order efficiency improvement can often be accomplished by matching each array element with a tuned line and an inductive or capacitive coupling element between adjacent array positions. The values can be selected by making a good engineering guess based on the active impedance ranges. If theoretical maximum efficiencies are to be approached, it is usually necessary to make extensive use of a digital computer in the design. An outline of such a computer program is given in this chapter.

A. Edelberg and Oliner Baffles to Modify Array Environment

In this early approach Edelberg and Oliner [23] experimentally leveled the variations in active driving element impedance with scan angle by placing metal fences between rows of elements in a large array of dipoles above a ground plane. The fence width and its height above the ground plane were varied until an experimental optimum combination was determined. Note that they placed the fences and worked to improve E-plane scan, which for dipoles in the array is much worse than H-plane scan variations. Some of their results are plotted in Fig. 33 below. Observe that

generator VSWR was reduced from about 4 to less than 1.3 for E-plane scan out to 60°.

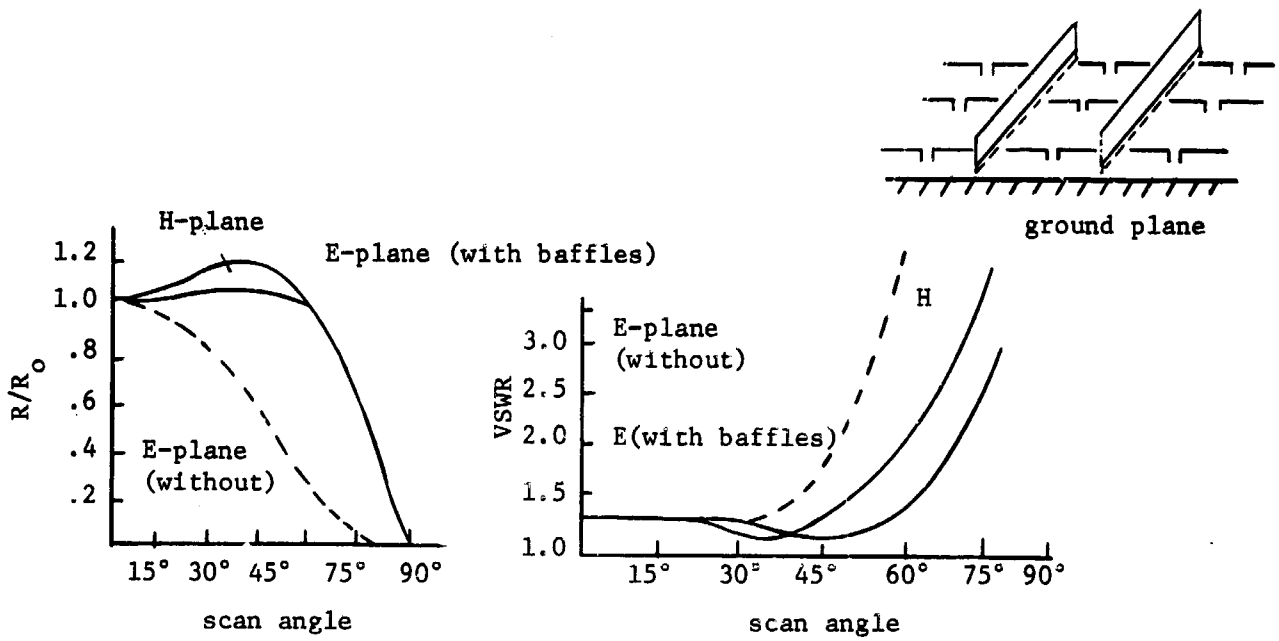

Fig. (a) Resistance vs Scan

Fig. (b) VSWR vs Scan Angle

Fig. 33 Effect of Fences on an Array of Dipoles

B. Impedance Matching with Scan Angle Using Connecting Circuits [26]

The following developments of Hannan et al. [26] illustrate the origins of the phase dependent reactance terms introduced by interconnecting adjacent array elements with reactive circuits. Since these reactances are lossless and can be shown to load each drive element with a reactive equivalent circuit which varys with the phasings of the drive generators, they can often by chosen to effectively offset array impedance variations with scan angle with no loss in radiated power. The connecting circuits introduce into each element line a signal which varies with generator phasing and hence scan angle. By proper selection, these networks can significantly reduce element mismatch over a

range of scan angles without sacrificing array gain.

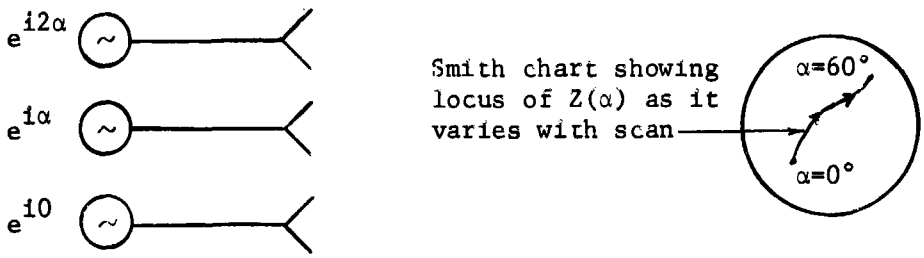

Fig. 34 No Compensation

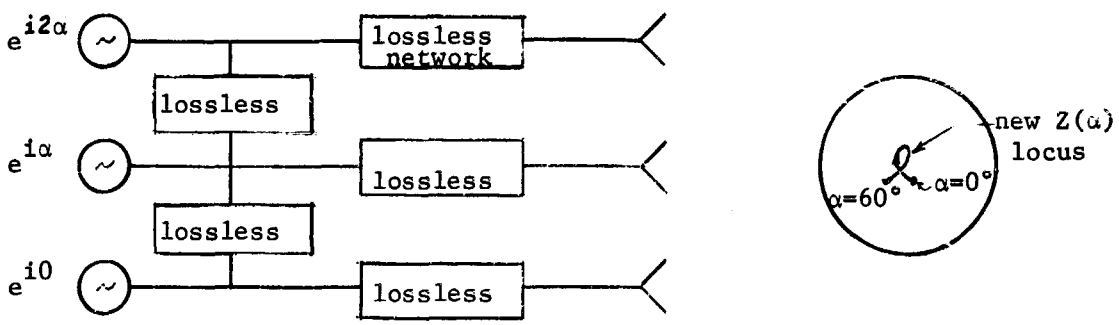

Fig. 35 With Connecting Circuit Matching

For the purpose of analysis it will be assumed that the arrays are infinite and regular. This means that the generators and elements have identical environments. It is found that the behavior of many finite arrays with a small number of elements can be treated as infinite arrays provided correction is made for edge effects.

1. Linear Array

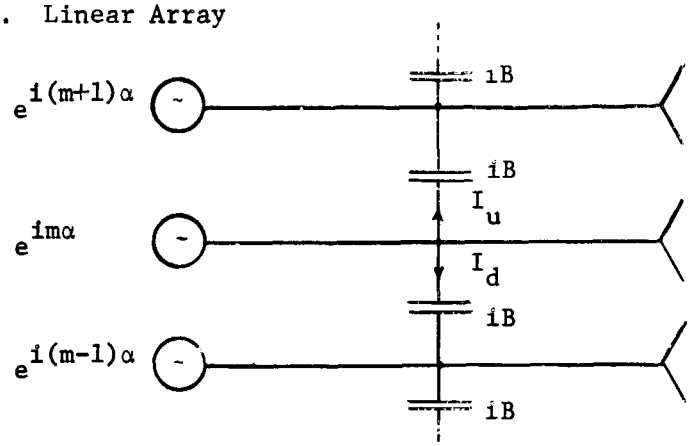

Fig. 36 Connecting Circuits in an Infinite Linear Array

Consider the effect of shunt susceptances connecting the element lines in the infinite linear array illustrated in Fig. 36. The net susceptance shunting the line to ground is found in the following manner:

$$I_s = I_u + I_d = iB\,[V_m - V_{m+1}] + iB\,[V_m - V_{m-1}] \qquad (5\text{-}1)$$

$$Y_{eq} = iB\,[2 - \frac{V_{m+1}}{V_m} - \frac{V_{m-1}}{V_m}] = \frac{I_s}{V_m} \qquad (5\text{-}2)$$

For an array phased to point in the θ_s-direction

$$\frac{V_{m+1}}{V_m} = e^{+i\alpha} \text{ and } \frac{V_{m-1}}{V_m} = e^{-i\alpha} \qquad (5\text{-}3)$$

where $\alpha = k\,d\,\sin\theta_s$ = progressive per element phase shift.

Substituting (5-3) into (5-2) gives

$$Y_{eq} = iB\,[2 - e^{i\alpha} - e^{-i\alpha}] = iB\,2[1 - \cos\alpha]. \qquad (5\text{-}4)$$

Using $\cos(\alpha) = 1-2\sin^2(\alpha/2)$ gives

$$Y_{eq} = i\ 4B \sin^2\left(\frac{\alpha}{2}\right). \tag{5-5}$$

Hence each line in the array is effectively shunted to ground by a susceptance

$$B_{eq} = 4\ B \sin^2\left[\frac{\alpha}{2}\right]. \tag{5-6}$$

The resultant equivalent circuits seen by the generators are shown below.

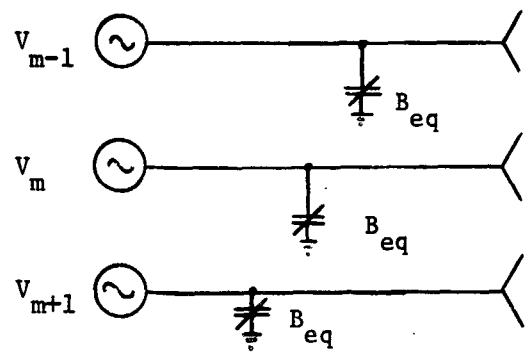

$$B_{eq} = 4B \sin^2\left[\frac{\alpha}{2}\right]$$

Fig. 37 Equivalent Array Networks

2. Planar Array

Row phase shift = β

Column phase shift = α

E-plane scan: $\pm\beta = kd \sin\theta$, $\alpha = 0$

H-plane scan: $\beta = 0$, $\alpha = \pm\ kd \sin\theta$

D-plane scan: $\pm\alpha = \pm \mp\beta = \frac{kd}{2} \sin\theta$

The effects of E-and H-plane connecting circuits:

E-plane: $B_{eq} = 4\, B_E \sin^2[\beta/2]$

H-plane: $B_{eq} = 4\, B_H \sin^2[\alpha/2]$

D-plane: $B_{eq}(E) = 4\, B_E \sin^2[\frac{\pi d \sin\theta}{2\lambda}]$.

Hannan et al.[26] worked out the case for a 7x9 array of $\lambda/2$ dipoles spaced with $d_x = d_y = \lambda/2$, a height of $\lambda/4$ above a ground plane. The original array for a $\pm 60°$ scan had a VSWR of 14 db (=5) and a maximum loss due to reflection of power of 2.6 db. With a first order simple compensation the VSWR was reduced to 4.5 db (1.68) and the reflection loss to 0.3 db. In this example, Hannan et al. used inductive coupling for H-plane compensation and capacitive coupling for E-plane compensation. The following steps which are illustrated in Fig. 38 are used in a typical matching procedure:

(1) A series network or a transmission line is adjusted to rotate the E-plane locus so that it can be offset with a susceptive shunt

(2) The scan dependent $B_{E_{eq}}$ is used to neutralize the above locus variation

(3) The H-plane locus is rotated to make it purely susceptive with scan

(4) $B_{H_{eq}}$ is added to cancel the susceptance in (3)

(5) The generator is impedance matched with 1_c and B_g.

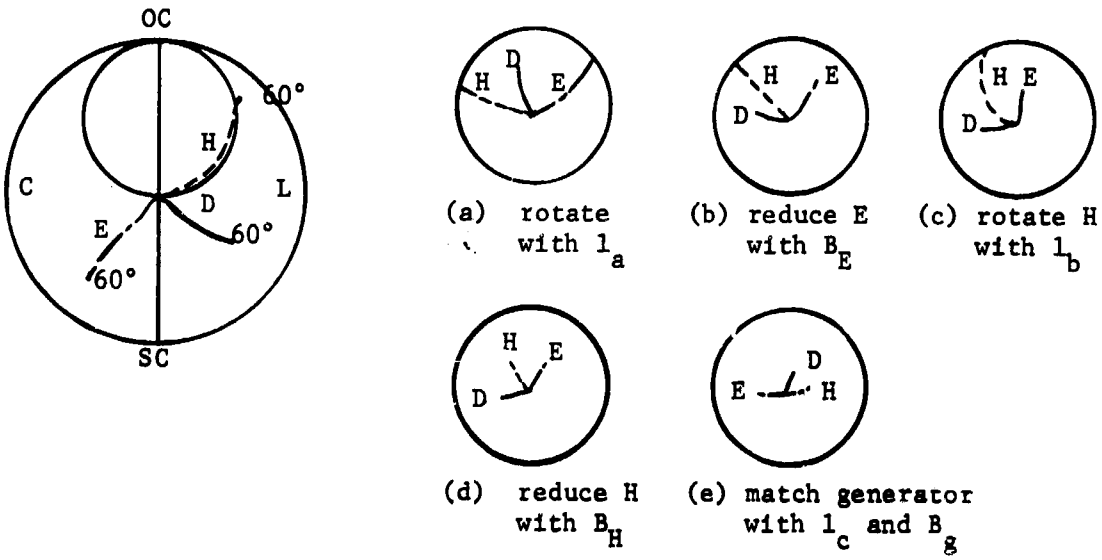

Fig. 38 Smith Chart Steps for a Typical Compensation

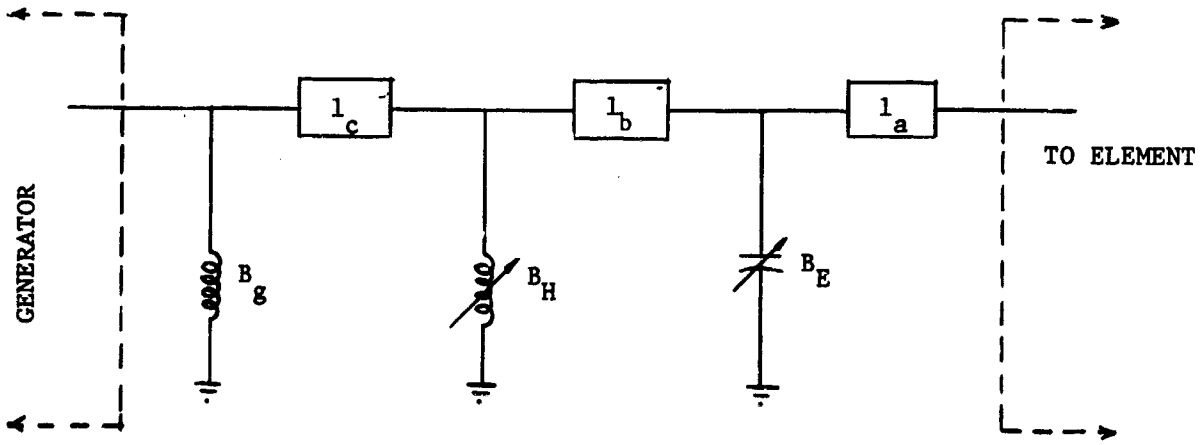

Fig. 39 Matching Network

C. COMPENSATION FOR WIDE ANGLE SCANS USING A DIELECTRIC SHEET IN FRONT OF THE ARRAY*[24]

This is a simple and possibly inexpensive compensation technique which, from a circuit and impedance matching point of view, has a lot in common with Hannan's method. Although the dielectric sheet method is fairly crude and somewhat restricted, it potentially yields a good trial and error means of improving the scan performance of a planar array.

For a thin dielectric sheet of thickness, t, and relative permittivity, ε_r, the effective broadside susceptance, B(0), is approximately

$$\frac{B(0)}{G_o} = (\varepsilon_r - 1)\,\frac{2\pi t}{\lambda_o} \tag{5-7}$$

so that within limits a desired susceptance can be obtained using a thickness

$$t = \frac{\lambda_o}{2\pi(\varepsilon_r - 1)}\,\frac{B(0)}{G_o} \tag{5-8}$$

The effective susceptance as a function of scan angle is given by

$$\text{H plane:}\quad \frac{B(\theta)}{B(0)} = \frac{1}{\cos\theta} \tag{5-9}$$

$$\text{E plane:}\quad \frac{B(\theta)}{B(0)} = \cos\theta - \frac{\sin^2\theta}{\varepsilon_r \cos\theta} \tag{5-10}$$

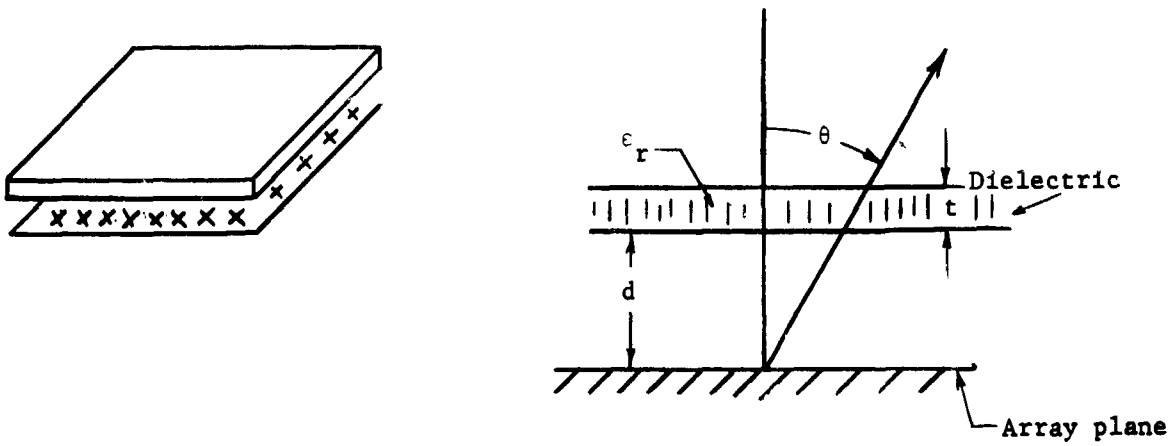

Fig. 40 Dielectric Sheet Above an Array

A rough outline of the basis of the compensation procedure is as follows:

1. The Smith chart locus of active impedance variations in the uncompensated array is examined as a function of scan plane and angle.
2. Height, d, of the dielectric sheet above the array plane (see Fig. 40) is chosen to rotate or shift the locus so that it has a susceptance portion which can be compensated.
3. Thickness, t, and dielectric constant, ε_r, are chosen to give the desired neutralization. Because of coupling wave effects, it is best to keep "t" small and work with ε_r.

Again note that the method readily lends itself to trail and error experimentation to improve usable scan range. The reflection coefficient at a central element could be monitored as a function of scan angle and the dielectric constant, the position, and the thickness can be changed to hopefully find a "best" combination to increase the limits of efficient scan.

Parad [29] shows that the surface wave velocity is strongly dependent on the dielectric thickness and is fairly independent of the dielectric constant for large ε_r. This, of course, implies that in order to avoid limits on scan angle imposed by coupling modes, it is best to keep the dielectric thin and work with ε_r to widen the scan range.

Because of the simplicity and inexpensiveness of the dielectric sheet compensation method, it is highly recommended whenever it will do the job. In general it works best for limited scans (up to $\pm$ 60° from broadside) where only an efficiency improvement and not ideal matching is required. The next few sections include some supplementary material that should be useful when applying this method. One section summarizes some of the important transmission and impedance characteristics of dielectric sheets, and the other deals with the limits on dielectric sheet matching posed by surface wave effects. Both qualitative and quantitative results are presented.

C.1. Impedance and Transmission Properties of Planar Dielectric Sheets

Summarized in this section are some of the formulas applying to the transmission of plane waves through infinite dielectric sheets. Most of the results are elementary ones which are taken from developments given in Collin [30] and Harrington [31].

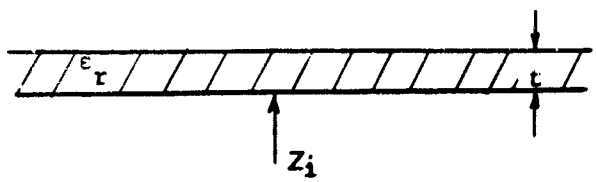

Fig. 41 Dielectric Sheet

Thin Dielectric Sheets

For normal incidence

$$Z_i = \eta_1 \frac{\eta_o \cos \beta t + i\, \eta_1 \sin(\beta t)}{\eta_1 \cos(\beta t) + i\, \eta_o \sin(\beta t)} \; ; \; Y_i = \frac{1}{\eta_1} \frac{\frac{1}{\sqrt{\varepsilon_r}} + i \tan(\beta t)}{1 + i \frac{1}{\sqrt{\varepsilon_r}} \tan(\beta t)} = G_o + iB_o \quad (5\text{-}11)$$

where

$$\eta_1 = \eta_o \frac{1}{\sqrt{\varepsilon_r}} = \sqrt{\frac{\mu_1}{\varepsilon_1}}$$

$$\eta_o = \sqrt{\frac{\mu_o}{\varepsilon_o}} = 377\Omega \qquad Y_i = \frac{1}{\eta_o} \frac{1 + \tan^2 \beta t + i \tan(\beta t)\left[\sqrt{\varepsilon_r} - \frac{1}{\sqrt{\varepsilon_r}}\right]}{1 + \frac{1}{\varepsilon_r} \tan^2 \beta t}$$

$$\beta = \frac{\omega}{v_1} = \omega \sqrt{\mu \varepsilon_1} = k_o \sqrt{\varepsilon_r}$$

If the thickness "t" is small ($\beta t \ll 1$)

$$Y_i \simeq \frac{1}{\eta_o} \frac{1 + i\sqrt{\varepsilon_r}\, \beta t}{1 + i \frac{1}{\sqrt{\varepsilon_r}} \beta t} = \frac{1}{\eta_o} \frac{1 + (\beta t)^2 + i\beta t\left(\sqrt{\varepsilon_r} - \frac{1}{\sqrt{\varepsilon_r}}\right)}{1 + \frac{(\beta t)^2}{\varepsilon_r}} \quad (5\text{-}12)$$

Thus

$$G_o \simeq \frac{1}{\eta_o} \quad (5\text{-}13)$$

$$B_o \simeq \frac{1}{\eta_o} k_o t(\varepsilon_r - 1) = G_o \frac{2\pi t}{\lambda_o} (\varepsilon_r - 1) \; . \quad (5\text{-}14)$$

For oblique incidence, the normalized susceptance of a thin dielectric sheet can be shown to vary as

H-plane: $$\frac{B(\theta)}{B_o} = \frac{1}{\cos\theta} \qquad (5\text{-}15)$$

E-plane: $$\frac{B(\theta)}{B_o} = \cos\theta - \frac{\sin^2\theta}{\varepsilon_r \cos\theta}. \qquad (5\text{-}16)$$

These variations are graphically presented in Fig. 42 below.

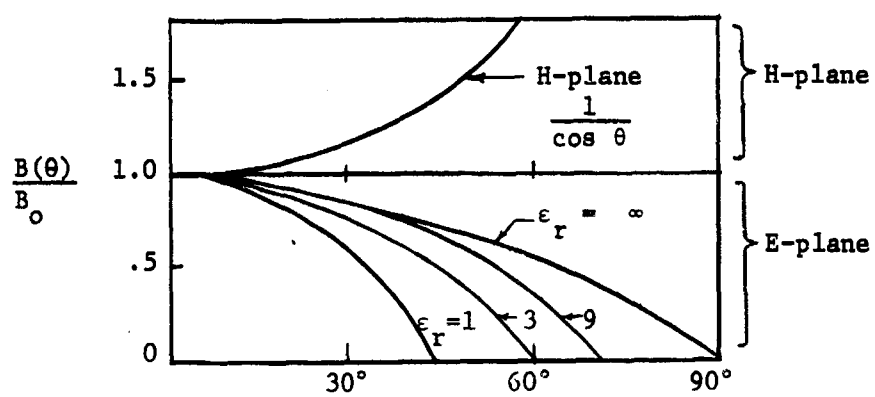

Fig. 42 Normalized Susceptance of a Thin Dielectric Sheet

Observe that the H-plane susceptance increases with θ and the E-plane susceptance decreases with θ. Note also that in the E-plane $B(\theta)$ goes negative for

$$\tan\theta \geq \sqrt{\varepsilon_r}.$$

In order to illustrate some of the degrees of freedom and to emphasize the approximations involved in a typical dielectric matching scheme, the following developments for a dielectric sheet located at a height "d" above

an array plane will be repeated.

(a) H-plane scan (polarized perpendicular to the plane of incidence):

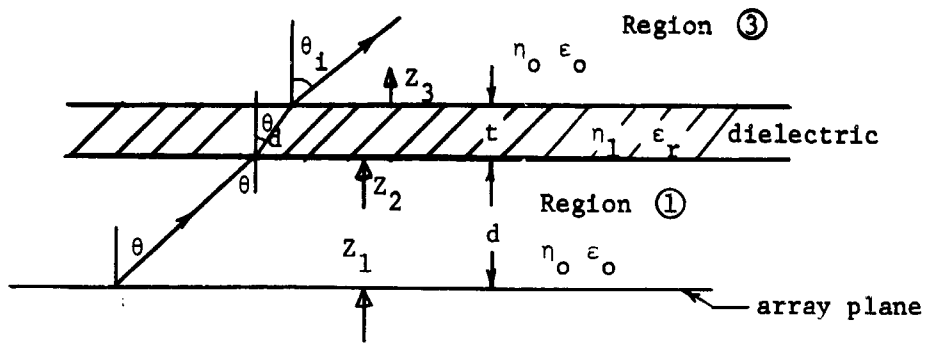

Fig. 43 Dielectric Sheet above a Planar Array-
Transmission Path

ε_r = relative dielectric constant

t = dielectric thickness

d = height of the dielectric above the reference plane

$$Z_3 = \frac{\eta_o}{\cos\theta_i} \tag{5-17}$$

$$\beta_1 = k_d \cos\theta_d = k_o\sqrt{\varepsilon_r}\cos\theta_d = k_o\sqrt{\varepsilon_r - \sin^2\theta_i} \tag{5-18}$$

Snell's Law:

$$\frac{\sin\theta_d}{\sin\theta_i} = \frac{v_d}{v_i} = \frac{1}{\sqrt{\varepsilon_r}} \tag{5-19}$$

$$Z_2 = \frac{\eta_1}{\cos\theta_d}\frac{Z_3 + i\frac{\eta_1}{\cos\theta_d}\tan(\beta_1 t)}{\frac{\eta_1}{\cos\theta_d} + i Z_3 \tan(\beta_1 t)} = \frac{\eta_1}{\cos\theta_d}\frac{\frac{\eta_o}{\cos\theta_i} + i\frac{\eta_1}{\cos\theta_d}\tan(\beta_1 t)}{\frac{\eta_1}{\cos\theta_d} + i\frac{\eta_o}{\cos\theta_i}\tan(\beta_1 t)}$$

$$= \frac{\eta_1}{\cos\theta_d}\frac{1 + i\frac{1}{\sqrt{\varepsilon_r}}\frac{\cos\theta_i}{\cos\theta_d}\tan(\beta_1 t)}{\frac{1}{\sqrt{\varepsilon_r}}\frac{\cos\theta_i}{\cos\theta_d} + i\tan(\beta_1 t)} \qquad (5\text{-}20)$$

$$Z_1 = \frac{\eta_o}{\cos\theta_i}\frac{Z_2 + i\frac{\eta_o}{\cos\theta_i}\tan(k_o\cos\theta_i d)}{\frac{\eta_o}{\cos\theta_i} + i Z_2 \tan(k_o d\cos\theta_i)} \qquad (5\text{-}21)$$

$$Z_2(\perp\text{pol.}) = \frac{\eta_o}{\sqrt{\varepsilon_r - \sin^2\theta}}\frac{1 + i\frac{\cos\theta}{\sqrt{\varepsilon_r - \sin^2\theta}}\tan(\beta_1 t)}{\frac{\cos\theta}{\sqrt{\varepsilon_r - \sin^2\theta}} + i\tan(\beta_1 t)} \equiv Z_2(H) \qquad (5\text{-}22)$$

Usual approximations: assume $\varepsilon_r \geq 2$, $k_o t \ll 1$, $\tan(\beta_1 t) \approx \beta_1 t$

$$Z_2(H) \approx \frac{\eta_o}{\sqrt{\varepsilon_r - \sin^2\theta}}\frac{1 + i\frac{\cos\theta}{\sqrt{\quad}}k_o t\sqrt{\quad}}{\frac{\cos\theta}{\sqrt{\quad}} + i k_o t\sqrt{\quad}} = \eta_o\frac{1 + i k_o t\cos\theta}{\cos\theta + i k_o t(\varepsilon_r - \sin^2\theta)}$$

$$Y_2(H) = \frac{1}{Z_2(H)} = \frac{1}{\eta_o}\frac{\cos\theta[1+(k_o t)^2(\varepsilon_r - \sin^2\theta)] + ik_o t(-\cos^2\theta + \varepsilon_r - \sin^2\theta)}{1 + (k_o t)^2\cos^2\theta} \qquad (5\text{-}23)$$

$$\approx \frac{1}{\eta_o}[\cos\theta(1+k_o^2 t^2)(\varepsilon_r - \sin^2\theta + ik_o t(\varepsilon_r - 1)]$$

where $\sqrt{\quad} = \sqrt{\varepsilon_r - \sin^2\theta}$

Referred to the direction of propagation in region ①

$$Y = \frac{Y_2}{\cos\theta} = G(\theta) + iB(\theta) = \frac{1}{\eta_o}\left[1+(k_o t)^2(\varepsilon_r-\sin^2\theta)+i\frac{k_o t(\varepsilon_r-1)}{\cos\theta}\right] \quad (5\text{-}24)$$

from which it is seen that

$$\frac{B(\theta)}{B_o} = \frac{1}{\cos\theta} \quad \text{where } B_o = \frac{k_o t(\varepsilon_r-1)}{\eta_o} \; . \quad (5\text{-}25)$$

(b) E-plane scan (polarized in the plane of incidence):

Here

$$Z_3 = \eta_o\cos\theta_i \; ; \; \beta_r = k_d\cos\theta_d = k_o\sqrt{\varepsilon_r - \sin^2\theta_i}$$

$$Z_2 = \eta_1\cos\theta_d\,\frac{Z_3+i\eta_1\cos\theta_d\tan(\beta_r t)}{\eta_1\cos\theta_d+iZ_3\tan(\beta_r t)} = \eta_1\cos\theta_d\,\frac{\eta_o\cos\theta_i+i\eta_1\cos\theta_d\tan(\beta t)}{\eta_1\cos\theta_d+i\eta_o\cos\theta_i}$$

$$= \eta_1\cos_d\,\frac{\sqrt{\varepsilon_r}\,\dfrac{\cos\theta_i}{\cos\theta_d} + i\tan\left(k_o\sqrt{\varepsilon_r-\sin^2\theta_i}\,t\right)}{1+i\sqrt{\varepsilon_r}\tan\left(tk_o\sqrt{\varepsilon_r-\sin^2\theta_i}\right)\dfrac{\cos\theta_i}{\cos\theta_d}} \quad (5\text{-}26)$$

For $k_o t \ll 1$ and $\varepsilon_r \geq 2$,

$$Z_2 \simeq \frac{\eta_o}{\sqrt{\varepsilon_r}}\sqrt{1-\frac{1}{\varepsilon_r}\sin^2\theta_i}\;\frac{\dfrac{\sqrt{\varepsilon_r}\cos\theta_i}{\sqrt{1-\frac{1}{\varepsilon_r}\sin^2\theta_i}} + i\,k_o\sqrt{\varepsilon_r-\sin^2\theta_i}\;t}{1+i\sqrt{\varepsilon_r}\,k_o t\sqrt{\varepsilon_r-\sin^2\theta_i}\,\dfrac{\cos\theta_i}{\sqrt{1-\frac{1}{\varepsilon_r}\sin^2\theta_i}}}$$

$$Z_2(E) \simeq \eta_o\,\frac{\cos\theta_i + i\,k_o t\left(1-\frac{\sin^2\theta}{\varepsilon_r}\right)}{1+i\,k_o t\,\varepsilon_r\cos\theta_i} \quad (5\text{-}27)$$

$$Y_2(E) \approx \frac{1}{\eta_o} \frac{\frac{1}{\cos\theta}\left[1+(k_o t)^2\,\varepsilon_r\left(1-\frac{\sin^2\theta}{\varepsilon_r}\right)\right]+ik_o t\left[\varepsilon_r-\frac{1}{\cos^2\theta}\left(1-\frac{\sin^2\theta}{\varepsilon_r}\right)\right]}{1+(k_o t)^2\,\frac{1}{\cos^2\theta}\left[1-\frac{\sin^2\theta}{\varepsilon_r}\right]^2} \qquad (5\text{-}28)$$

and thus

$$B_o \approx \frac{1}{\eta_o}\frac{k_o t(\varepsilon_r - 1)}{1+(k_o t)^2} \approx \frac{1}{\eta_o} k_o t(\varepsilon_r - 1) \qquad (5\text{-}29)$$

Ignoring the contribution of the second term in the denominator and referring the admittance to the direction of propagation [i.e., $Y = \cos\theta\, Y_2(E)$] yields

$$G(\theta) \approx \frac{1}{\eta_o}\left[1+(k_o t)^2\,\varepsilon_r\left(1-\frac{\sin^2\theta}{\varepsilon_r}\right)\right] \qquad (5\text{-}30)$$

$$B_o = \frac{k_o t}{\eta_o}(\varepsilon_r - 1) \qquad (5\text{-}31)$$

$$\frac{B(\theta)}{B_o} = \cos\theta - \frac{\sin^2\theta}{\varepsilon_r\cos\theta} \qquad (5\text{-}32)$$

C.2. Qualitative Results for Arrays Covered With Dielectric Sheets or Dielectric Element Plugs

(1) Generally speaking resonant peaks of reflection coefficient occur at scan angles between the angles of formation expected for the grating lobe for the dielectric and that of the grating lobe for air. (Knittel)[16] The following are observations of Wu and Galindo [32,33] which are based on their comparison of scan properties of parallel-plate waveguides loaded with dielectric plugs with their earlier (Jan. '68) loading with a

dielectric sheet (rectangular array).

(2) The radiation properties of an array can be substantially changed by covering it with a dielectric sheet. Typically such coverings introduce resonant peaks in the plot of reflection coefficient, Γ, versus scan angle. Frequently $\Gamma \to 1$ prior to the angle predicted by the occurrence of a grating lobe.

(3) For thin enough slabs no reflection peaks are observed.

(4) For slab thicknesses greater than certain critical values of the order of $\frac{3}{16}\lambda_e$ (λ_e = wavelength in the dielectric) resonant peaks begin to occur. At the threshold thickness the resonant peak is near the grating lobe formation angle. According to Wu and Galindo if $\frac{1}{2} < d/\lambda < 1$, $\theta_{cr} \simeq \frac{2\pi}{1 - (d/\lambda)}$.

(5) For sheets with fixed element spacing, d, and dielectric constant, ε_r, the resonant peaks migrate toward broadside as the slab thickness is increased.

(6) More than one peak may occur if the thickness of the slab is large enough, say greater than $\frac{3}{4}\lambda_e$.

(7) Normally resonant peaks correspond to complete reflection where the reflection coefficient is unity.

(8) Dielectric plugs can, but do not always, give rise to resonant peaks in Γ.

(9) While dielectric sheets invariably cause peaks if the thickness exceeds a certain value, such is not the case for plugs in waveguides.

(10) Exterior sheets may give rise to more than one peak if they are thick enough; however, Wu and Galindo have not observed any multiple peaks for plugs.

(11) As a general rule $\Gamma(\theta)$ is flatter with plugs than for waveguides loaded with dielectric sheets implying a possible better impedance and efficiency match. Both sheets and plugs can be used to improve efficiency.

C.3. Input Admittance to a Slot Array Covered by a Dielectric Sheet

This section is a strengthening of the work of Parad [29] that applies to an infinite array of short slots covered by a dielectric sheet. In it expressions for the admittance variations with E-plane scan are derived. An important consequence of the analysis is the observation that dielectric thickness, not dielectric constant, is the important factor in determining surface wave velocity. Thus, when using the dielectric sheet method for match compensation, it is recommended that the sheet be kept thin and the dielectric constant be selected to give the desired match.

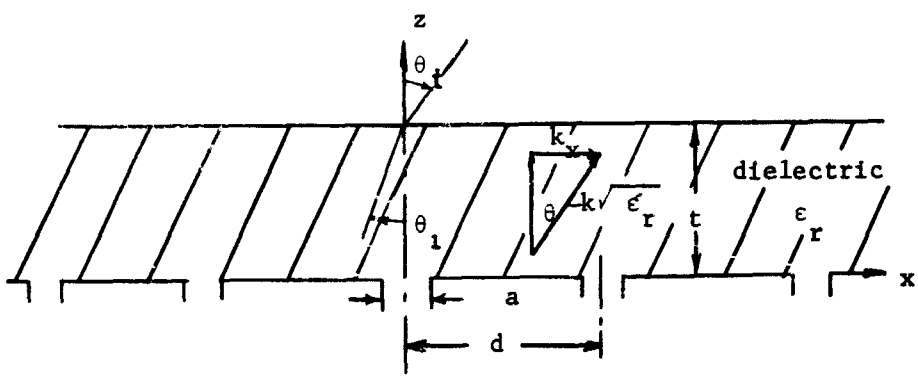

Fig. 44 Dielectric Covered Slots

Figure 44 shows a set of narrow slots of width "a", located in xy-plane and extending to infinity in the y-direction. For such narrow slots, it is assumed that E_x is a constant independent of x across their

width. The array is steered in the θ-direction by feeding the slots with a progressive phase shift

$$\delta = v_o d = k_x d \tag{5-33}$$

where d = slot spacing and k_x = x-directed phase constant of the slot feed system. Beam maximums occur when $\psi = kd \sin\theta - \delta = 0 \pm 2n\pi = kd \sin\theta - k_x d$, and the following relations apply to a propagating wave:

$$\sin\theta = k_x/k$$

$$k_x = v_o \pm 2n\pi d$$

$$\cos\theta = \sqrt{1 - (k_x/k)^2}$$

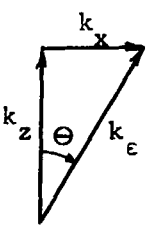

Method:

1. Express field at z = 0 as a sum of an infinite number of plane waves
2. Determine the input admittance at z = 0 for a plane wave
3. Compute the total input power at z = 0 for an aperture of unit width in the y-direction and length, d, in the x-direction
4. Express the input admittance in terms of the input power and voltage.

As is now well known, this geometry can be described by a Floquet series [40] which is just a Fourier Series for $E_x(x,o)$ which is modified with a phase taper term to account for the progressive phase excitation [Replaces Eqs. (2), (3), (4), in Parad's proof] of the slots necessary for pointing the beam.

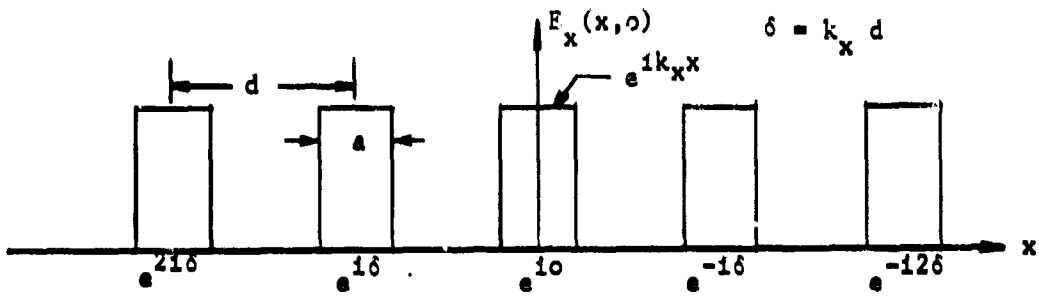

Fig. 45 Slot Illumination

A mathematical expression for a periodic aperture distribution with a phase tapered excitation is found by

(1) Writing a Fourier series for the pulses that includes a phase taper $k_x x$ on the center element.

(2) Multiplying the periodic series found in (1) by a phase taper term $-k_x x$.

The phase tapers (1) and (2) combine to produce a net phase term for the nth element of e^{-jndk_x}

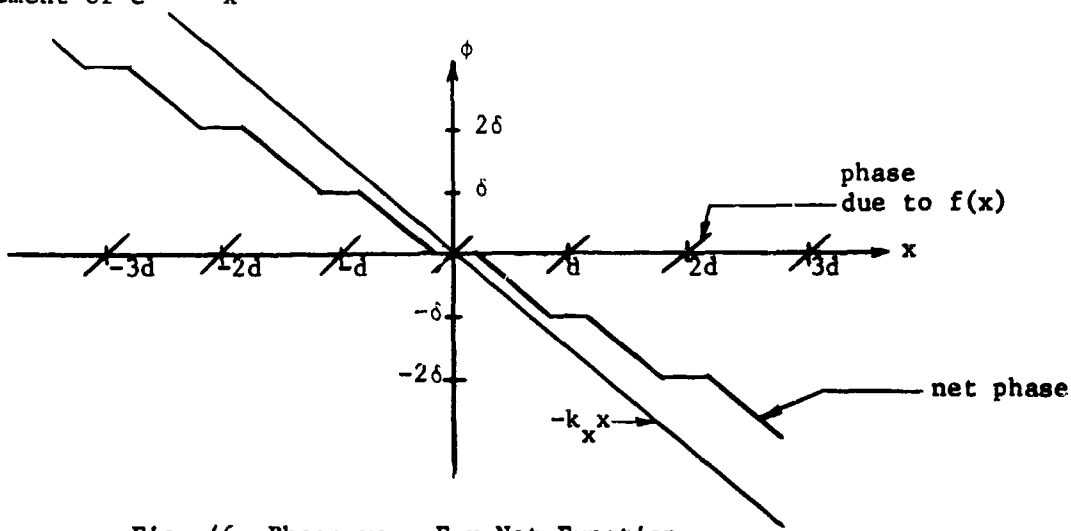

Fig. 46 Phase vs x For Net Function

For the example of the above slots the periodic function is:

$$f(x) = \sum_{-\infty}^{\infty} C_n e^{-j2\pi nx/d} \tag{5-34}$$

$$C_n = \frac{1}{d} \int_{-a/2}^{a/2} e^{jk_x x + j2\pi nx/d} = \frac{a}{d} \frac{\sin[\frac{a}{2}(k_x + 2\pi n/d)]}{\frac{a}{2}[k_x + 2\pi n/d]} \tag{5-35}$$

$$f(x) = \frac{a}{d} \sum_{-\infty}^{\infty} \frac{\sin[\frac{a}{2}(k_x + 2\pi n/d)]}{\frac{a}{2}(k_x + 2\pi n/d)} e^{-j2\pi nx/d} \tag{5-36}$$

Now adding the phase taper factor gives the net series

$$E_x(x,o) = e^{-jk_x x} f(x) = \frac{a}{d} \sum_{-\infty}^{\infty} \frac{\sin[\frac{a}{2}(k_x + 2\pi n/d)]}{\frac{a}{2}(k_x + 2\pi n/d)} e^{-ix(k_x + 2\pi n/d)} \tag{5-37}$$

As with most series solutions the above masks the physical significance of the apertures, however, the form of the series suggests a sum of plane waves, the nth having an amplitude equal to C_n.

The input power to a section of width, d, and length, L, (in the y-direction) is

$$P = \frac{1}{2} \int_0^L \int_{-d/2}^{d/2} E_x H_y^* \, dx dy = \frac{L|E|^2}{2} \left(\frac{a}{d}\right)^2 \int_{-d/2}^{d/2} \sum_n \frac{\sin(\,)}{(\,)} e^{-j2\pi nx/d}$$

$$\sum_m Y_{im}^* \frac{\sin(\,)}{(\,)} e^{+j2\pi mx/d} \, dx \tag{5-38}$$

where Y_{im} = input admittance of the mth wave

$$Y_i = \frac{H_y}{E_x} = \frac{1}{n\cos\theta} = \frac{1}{n\sqrt{1-k_v^2/k^2}} \tag{5-39}$$

All integrals in (5-38) are zero except when m = n giving

$$P = \frac{a^2 L|E|^2}{2d} \sum_{-\infty}^{\infty} Y_{in}^* \frac{\sin^2[\frac{a}{2}(k_x+2\pi n/d)]}{[\frac{a}{2}(k_x+2\pi n/d)]^2} \tag{5-40}$$

Also

$$P = \frac{1}{2} VI^* = \frac{1}{2}(Ea)(Ea)^*Y^* = \frac{1}{2} a^2 |E|^2 Y^* \tag{5-41}$$

Thus

$$Y = \frac{2P^*}{a^2|E|^2} = \frac{L}{d} \sum_{-\infty}^{\infty} Y_{in} \frac{\sin^2[\frac{a}{2}(k_x+2\pi n/d)]}{[\frac{a}{2}(k_x+2\pi n/d)]^2} \tag{5-42}$$

where Y_{in} = input admittance to the nth plane wave at the surface z = 0

By (5-39) it follows that

$$Y_{in} = \frac{1}{n\sqrt{1-(\frac{v_o+2\pi n/d}{k})^2}} \tag{5-43}$$

When the array is covered by a dielectric of thickness, t, and relative permittivity, ϵ_r, the admittance seen looking into the sheet is

$$Y_{in} = Yon \frac{Yln + jYon \tan(\beta_n t)}{Yon + jYln \tan(\beta_n t)} \tag{5-44}$$

where

$$Yon = \frac{H_{y_i}}{E_{x_i}}\Big|_n = \frac{1}{\eta\cos\theta_{in}} = \frac{\frac{\sqrt{\varepsilon_r}}{\eta_o}}{\sqrt{1 - \frac{1}{\varepsilon_r k_o^2}(v_o + 2\pi n/d)^2}} \qquad (5\text{-}45)$$

$$Yin = \frac{1}{\eta_o \cos\theta_t} = \frac{1}{\eta_o\sqrt{1 - (\frac{v_o + 2\pi n/d}{k_o})^2}} \qquad (5\text{-}46$$

$\beta n = \sqrt{\varepsilon_r}\, k \cos\theta_{in}$

θ_t = angle ray leaves dielectric surface = realized scan angle.

Observations:

1. From (5-42) the admittance Y has a pole where Y_{in} has a pole. It is theoretically possible to eliminate such poles by using a different aperture distribution.
2. From (5-44) it is seen that these poles can first occur when θ_t is imaginary (no radiation) corresponding to the excitation of surface wave modes.
3. For a thin dielectric layer, tan $\beta t \simeq \beta t$ and a pole in (5-44) occurs when

$$Y_{on} + jY_{1n}\beta t = 0 \rightarrow \frac{\sqrt{\varepsilon_r}}{\cos\theta_{in}} = -j\,\frac{\sqrt{\varepsilon}\, kt\cos\theta_{in}}{\cos\theta_{1n}}$$

$$\cos\theta_{1n} = -j\,kt\cos^2\theta_{in} = \sqrt{1 - k_v^2/k^2} = -jkt(1 - k_v^2/\varepsilon_r k^2)$$

Solving for k_v^2 yields

$$\frac{k_v^2}{k^2} = \varepsilon_r + \frac{\varepsilon_r^2}{2k^2t^2}\left[1 - \sqrt{1 + 4k^2t^2\frac{\varepsilon_r - 1}{\varepsilon_r^2}}\right] \qquad (5\text{-}47)$$

For $kt < \cdot 1$, Eq. (5-47) gives $\frac{k_v^2}{k^2} \approx 1 + k^2t^2\left(\frac{\varepsilon_r - 1}{\varepsilon_r}\right)^2$ (5-48)

which is nearly independent of dielectric constant ε_r.

4. The admittance pole occurs at scan angles prior to the grating lobes since Eq. (5-48) shows that the surface wave propagation constant is greater than that of free space (i.e., $k_v > k$).

D. Use of a Computer for Planar Array Match Compensation Through Adjacent Element Coupling [28]

Here a set of equations is developed which can be programmed on a digital computer for a systematic realization of Hannan's compensation technique. It assumes that the array coupling coefficients are either experimentally or theoretically known (normally coupling coefficients are easier to measure than active impedances), and it uses pi-type reactances for interconnecting adjacent element channels.

The required program inputs are

(1) Coupling coefficients, C_{mn}

(2) Shape of the scan region

(3) Grid structure

(4) Desired matching scheme

where the last three are design alternatives.

Hannan [34] has shown that by interconnecting all channels it is theoretically possible to impedance match an infinite phased-array antenna for all scan angles. In this development only adjacent channels (maximum of 8) are connected so that a perfect match is not expected. However, if enough care is taken, the results using this finite number

of couplings are excellent even for scans greater than $\pm$ 60°. As an indication of the possibilities of a truncated matching scheme, Amitay et al. [35] in a recent paper went a step farther and were successful in matching an array of circularly polarized elements out to $\pm$ 60° using only a lossless series matching obstacle behind each antenna element. Thus there are two choices for behind-the-array circuit matching. The general case consisting of a matching network behind each element and reactive couplers between contigious elements is the most powerful, and it is, therefore, recommended for wide angle scans or ones where high efficiency is needed. The other consists of the series network alone and shows promise for simple, non-critical compensations.

The array considered in this development is planar with a rectangular grid located in the xy-plane as shown in Fig. 47 below.

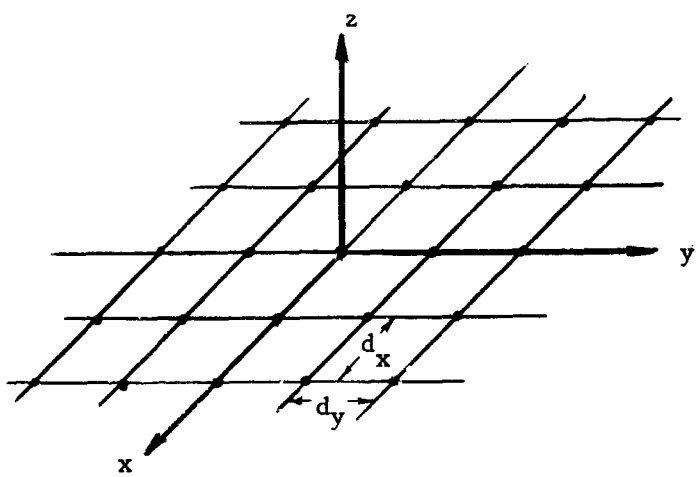

Fig. 47 Rectangular Grid Array

The elements have a uniform amplitude distribution and a progressive phase shift such that the excitation of the mnth element is

$$V_{mn} = V_o e^{im\psi_x + in\psi_y} \qquad (5\text{-}49)$$

where

$$\psi_x = kd_x \sin\theta \cos\phi$$

$$\psi_y = kd_y \sin\theta \sin\phi. \qquad (5\text{-}50)$$

By reciprocity the coupling coefficients between the 00th and the mnth elements are equal

$$C_{mn}^{oo} = C_{oo}^{mn} = C_{mn} = |C_{mn}| \, e^{i\Delta mn} \qquad (5\text{-}51)$$

and thus, if all the array elements are excited, the total reflected voltage at the 00th element is given by

$$V_r = V_1 \sum\sum_{mn} C_{mn} \, e^{im\psi_x + in\psi_y}. \qquad (5\text{-}52)$$

The reflection coefficient referred to the plane of the array (see Fig. 49) is then

$$q = \frac{Vr}{V_1} = \sum\sum C_{mn} \, e^{im\psi_x + in\psi_y}. \qquad (5\text{-}53)$$

Observe that q is a function of ψ_x and ψ_y. Again this analysis assumes that the array has enough elements to approximate an infinite one. Of an extremely important practical nature is the fact that Wu and Galindo [36,37] and others [13,38] have shown that a moderate number of array coupling coefficients (on the order of 11x11 to 13x13) are often sufficient to describe a central element's behavior with reasonable accuracy. As a consequence, only a finite number of coupling coefficients need be measured when using this particular method for design purposes.

The most general case to be treated is shown in Fig. 48, and it allows for coupling between an element and its eight immediate neighbors

in a rectangular grid with reactive pi-networks for coupling. Note that the assumed symmetry reduces the unknown coupling admittances to four: Y_t, Y_2, Y_4 and Y_6.

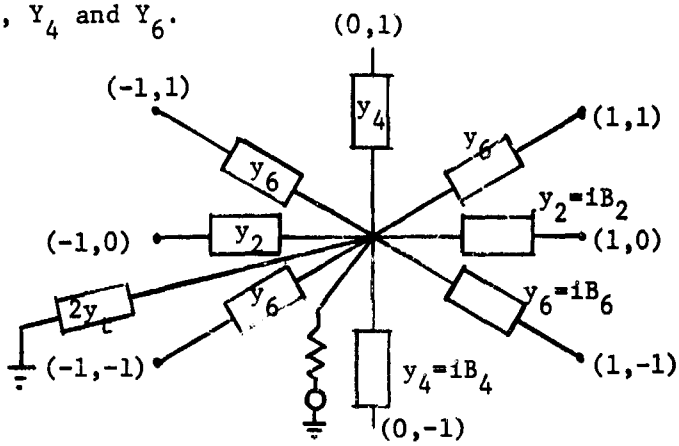

Fig. 48 Matching Element Geometry

The basic feed connecting system is illustrated in Fig. 49 below

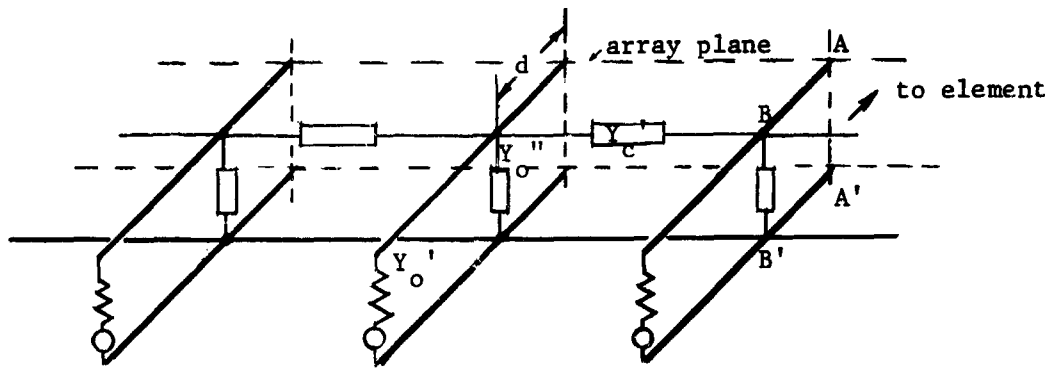

Fig. 49 Compensation Coupling Model

where AA' = array plane

BB' = coupling junction plane where the generator line, the array element line, and the coupling networks meet.

Y_c = effective admittance at BB' of the coupling networks

Y_o'' = characteristic admittance of the array line

Y_o' = characteristic admittance of the generator line

The phase shift between AA' and BB' is

$$\frac{\phi}{2} = k''d = \frac{2\pi d}{\lambda}$$

and hence the reflection coefficients referred to the coupling junction plane, BB', is given by

$$q'' = e^{-i\phi}\, q = e^{-i\phi} \sum\sum_{mn} Cmn\ \ e^{im\psi_x + in\psi_y}. \tag{5-54}$$

Using the fact that

$$\Gamma = q = \frac{1 - y}{1 + y} \tag{5-55}$$

$$y = \frac{1 - q}{1 + q} = \text{normalized admittance}, \tag{5-56}$$

it follows that the active admittance at BB' looking into the line from the array element can be written

$$Y_L = Y_o'' \frac{1 - q''}{1 + q''} \tag{5-57}$$

Then the admittance at BB' due to the element line and the coupling network is

$$Y = Y_c + Y_L, \tag{5-58}$$

and the reflection coefficient seen by the generator line at BB' is

$$q_B = \frac{1 - Y/Yo'}{1 + Y/Yo'} \tag{5-59}$$

Since the voltages at BB' have the same relative phases as the generator voltages, Vmn, they can be written

$$Vmn' = Vo' e^{im\psi_x + in\psi_y} \tag{5-60}$$

and thus the total current into Y_c can be expressed as

$$\frac{Ic}{Vmn} = Y_2(1 - e^{i\psi_x}) + Y_2(1 - e^{-i\psi_x}) + Y_4(1 - e^{i\psi_y}) + Y_4(1 - e^{-i\psi_y})$$
$$+ Y_6[1 - e^{i\psi_x + i\psi_y} + 1 - e^{-i\psi_x - i\psi_y} + 2 - e^{i\psi_x - i\psi_y} - e^{-i\psi_x + i\psi_y}] + 2Y_t \tag{5-61}$$

$$Y_c = \frac{Ic}{Vmn} = 2[Y_2 + Y_4 + 2Y_6 + Y_t] - 2Y_2 \cos(\psi_x) - 2Y_4 \cos\psi_y - 2Y_6 \cos(\psi_x + \psi_y)$$
$$- 2Y_6 \cos(\psi_x - \psi_y) \tag{5-62}$$

In order to make some of the subsequent expressions notationally simpler, it is found convenient to define the following normalized variables ($i = \sqrt{-1}$)

$$iN_c = \frac{Yc}{Y_o'};\ iN_t = \frac{Y_t}{Y_o'};\ iN_2 = \frac{Y_2}{Y_o'};\ iN_4 = \frac{Y_4}{Y_o'};\ iN_6 = \frac{Y_6}{Y_o'};\ N_o = \frac{Y_o''}{Y_o'} \tag{5-63}$$

The reflection coefficient q_B is, of course, a measure of the effective system match. To optimally select the compensation circuit, a cost factor

$$CF = \int\int_{\text{scan region}} |q_B|^2 \, d\psi_x \, d\psi_y =$$
$$\int\int \left| \frac{1 - Y/Y_o'}{1 + Y/Y_o'} \right|^2 d\psi_x \, d\psi_y \tag{5-64}$$

is suggested. Ideally $y \triangleq \frac{Y}{Y_o'} = 1$ for the total scan range corresponding to CF = 0. For only a finite number of connecting elements it is assumed

that y in the compensated system is close to one and hence the approximation

$$\left|\frac{1-y}{1+y}\right|^2 \simeq \left|\frac{1-y}{2}\right|^2$$

can be used to put Eq. (5-64) in a more usuable form

$$CF \rightarrow I = \int\int_{\text{scan region}} |1-y|^2 \, d\psi_x \, d\psi_y \tag{5-65}$$

Then (1-y) is linearly related to N_o, N_t, N_2, N_4 and N_6 and

$$\frac{\partial I}{\partial N_o} = 0, \frac{\partial I}{\partial N_t} = 0, \cdots, \frac{\partial I}{\partial N_6} = 0 \tag{5-66}$$

are the conditions required to minimize I. The optimum values of the network sequence {N} are obtained by repeated solutions of (5-66) for various values of ϕ. The integral to be minimized is

$$I = \int\int_{\text{scan region}} |1-y|^2 \, d\psi_x \, d\psi_y \tag{5-67}$$

where in terms of the ratio definitions given in (5-63)

$$y = \frac{Y_c+Y_L''}{Y_o'} = i\Big(2(N_2+N_4+2N_6+N_t)-2N_2\cos(\psi_x)-2N_4\cos(\psi_y)-2N_6\cos(\psi_x+\psi_y)$$

$$-2N_6\cos(\psi_x-\psi_y)\Big) + N_o\frac{1-q''}{1+q''} \tag{5-68}$$

Using (5-54) for q" it is seen that the last term in (5-68) becomes

$$N_o \frac{1-e^{-i\phi}\sum\sum C_{mne}^{im\psi_x + in\psi_y}}{1+e^{-i\phi}\sum\sum C_{mne}^{im\psi_x + in\psi_y}} \tag{5-69}$$

which, since it is a doubly periodic function of ψ_x and ψ_y, can be expanded as

$$N_o \frac{1-q''}{1+q''} = N_o \left[1-2\sum\sum D_{mn}\, e^{im\psi_x+n\psi_y}\right] \tag{5-70}$$

Hence

$$1 - y = 1-N_o+2N_c\sum\sum D_{mn} e^{im\psi_x+in\psi_y} -i \left[2\,(N_t + N_2 + N_4 + 2N6)\right.$$

$$\left. - 2N_2\cos\psi_x - 2N_4\cos\psi_y - 2N_6\cos(\psi_x+\psi_y) - 2N_6\cos(\psi_x-\psi_y)\right]. \tag{5-71}$$

Amitay then used (5-66), (5-67), and (5-71) to obtain the following equations.

From $\partial I/\partial N_o = 0$,

$$a_{oo} - 2\sum\sum_{mn} D_{mn}'\, a_{mn} = N_o[a_{oo}-4\sum\sum_{mn} D_{mn}'\, a_{mn} + \sum\sum\sum\sum_{mnpq} D_{mn}\, D^*_{pq}\, a_{m-p,n-q}\,]$$
$$-4\,N_T\sum\sum_{mn} D_{mn}''\, a_{mn} + 2N_2\sum\sum D_{mn}''(a_{m+1,n} - 2a_{mn} + a_{m-1,n})$$
$$+2\,N_6\sum\sum D_{mn}''(a_{m+1,n+1} + a_{m-1,n+1} + a_{m+1,n-1} + a_{m-1,n-1} - 4a_{mn}) \tag{5-72}$$

From $\partial I/\partial N_t = 0$,

$$0 = -N_o\sum\sum D_{mn}''a_{mn} + N_t a_{oo} + N_2(a_{oo} - a_{10}) + N_4(a_{oo}-a_{01})+2N_6(a_{oo}-a_{11}) \tag{5-73}$$

From $\partial I/\partial N_2 = 0$

$$0 = N_o\sum\sum_{mn} D_{mn}''(a_{m+1,n}+a_{m-1,n}-2a_{mn}) + 2N_t(a_{oo}-a_{10}) + N_2(3a_{oo}+a_{20}-4a_{10})$$
$$+ 2N_4(a_{oo}+a_{11}-a_{10}-a_{01}) + 2N_6[2(a_{oo}-a_{10}) + a_{21} + a_{01} - 2a_{11}] \tag{5-74}$$

From $\partial I/\partial N_6 = 0$,

$$0 = N_o\sum\sum D_{mn}'(a_{m+1,n+1} + a_{m-1,n+1} + a_{m+1,n-1} + a_{m-1,n-1} - 4a_{mn})$$
$$+ 4N_t(a_{oo}-a_{11}) + 2N_2[2(a_{oo}-a_{11}) + a_{01} + a_{21} - 2a_{10}]$$
$$+ N_4[2(a_{oo}-a_{11}) + a_{10}+a_{12}-2a_{01}] + 2N_6[5a_{oo}+a_{02}+a_{20}+a_{22}-8a_{11}]. \quad (5\text{-}75)$$

From $\partial I/N_4 = 0$,

$$0 = N_o\sum\sum D_{mn}''(a_{m,n+1}+a_{m,n-1}-2a_{mn})+2N_t(a_{oo}-a_{01})+2N_2[a_{oo}+a_{11}-a_{01}-a_{10}]$$
$$+ N_4[3a_{oo}+a_{02}-4a_{01}]+2N_6[2(a_{oo}-a_{01})+a_{10}+a_{12}-2a_{11}]. \quad (5\text{-}76)$$

Note that in the above equations,

$$D_{mn}' = \text{Real}[D_{mn}]$$
$$D_{mn}'' = \text{Imag}[D_{mn}] \quad (5\text{-}77)$$

and

$$a_{mn} = \int\int_{\text{scan region}} e^{im\psi_x+in\psi_y}\, d\psi_x\, d\psi_y. \quad (5\text{-}78)$$

Furthermore, Eqs. (5-72) through (5-76) assume that a_{mn} is real. With a little additional bookkeeping one could allow for a complex a_{mn}; however, this is usually not necessary since a_{mn} are real for the commonly encountered cases of elliptical and rectangular scan regions such as sketched in Fig. 50.

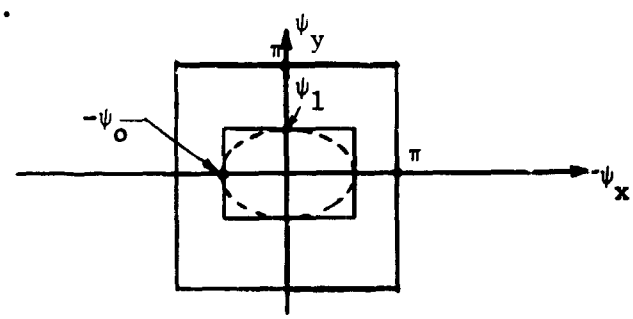

Fig. 50 Unit Cell With Elliptical and Rectangular Scan Regions

It is easily shown for the rectangular scan region that

$$a_{mn} = 4 \frac{\sin[m\psi_o] \sin[n\psi_1]}{m\ n} \tag{5-79}$$

and for the elliptical region,

$$a_{mn} = 2\pi\psi_o\psi_1 \frac{J_1[\sqrt{(m\psi_o)^2+(n\psi_1)^2}]}{\sqrt{(m\psi_o)^2+(n\psi_1)^2}} \tag{5-80}$$

Amitay used this method on a linearly polarized array of square waveguides spaced with $d/\lambda = .5714$. For a scan of $\pm$ 45° without any compensation, the returned power was as high as 30%. Using compensation within each channel but letting the adjacent channel coupling be zero ($N_2 = N_4 = N_6 = 0$), the returned power was reduced to around 5% over most of the scan region. For his final comparison Amitay [28] added interelement coupling ($N_o = 1$, $N_t = 0.512$, $N_2 = -0.0976$, $N_4 = -0.189$, $N_6 = 0$), and obtained a returned power that was under 1% for most of the scan region.

REFERENCES

1. R. C. Hansen, ed., Microwave Scanning Antennas, Vol. II, Academic Press, 1966, Chapter 1.

2. E. D. Sharpe, "A triangular arrangement of planar-array elements that reduces the number needed," IRE Trans. AP, March, 1961, pp. 126-129.

3. W. K. Kahn, "Ideal efficiency of a radiating element in an infinite array," IEEE Trans. AP, AP-15, July, 1967, pp. 534-538.

4. R. C. Hansen, ed., Microwave Scanning Antennas, Vol. II, Academic Press, 1966, Chapters 2 and 3.

5. J. L. Allen and B. L. Diamond, "Mutual coupling in array antennas," MIT Lincoln Lab., Lexington, Mass., Technical Report 424, October 4, 1966.

6. Hansen, op. cit. (4), pp. 216-224.

7. Hansen, op. cit. (4), pp. 243-245.

8. Hansen, op. cit. (4), pp. 282-283.

9. J. L. Allen, "Antenna arrays: new applications for an old technique," IEEE Spectrum, November, 1964, pp. 115-130.

10. B. L. Diamond, "Phased array radar studies," MIT Lincoln Lab., Technical Report TR 381, 1965.

11. Wasylkiwskyj and Kahn, "Mutual coupling and element efficiency for infinite linear arrays," Proc. IEEE, November, 1968, pp. 1901-1907.

12. Hansen, op. cit. (4), pp. 209-217.

13. T. R. Debski and P. W. Hannan, "Complex mutual coupling measured in a large phased-array antenna," Microwave Journal, June, 1965, pp. 93-96.

14. Wasylkiwskyj and Kahn, op. cit. (11), p. 1903.

15. L. W. Lechtreck, "Effects of coupling accumulation in antenna arrays," Trans. AP, AP-16, January, 1968, pp. 31-38.

16. G. H. Knittel, A. Hessel, and A. A. Oliner, "Element pattern nulls in phased arrays and their relation to guided waves," Proc. IEEE, November, 1968, pp. 1822-1836.

17. E. D. Sharp, op. cit. (2), pp. 126-199.

18. N. Amitay, J. Cook, R. Pecina, and C. Wu, "On mutual coupling and matching conditions in large planar phased arrays," 1964 IEEE G-AP International Symposium Program and Digest, p. 154.

19. Farrel and Kuhn, "Mutual coupling effects of triangular-grid arrays of model analysis," Trans. AP, AP-14, September, 1966, pp. 652-654.

20. Lechtreck, op. cit. (15), pp. 31-38.

21. G. H. Knittel, "Choosing the number of faces of a phased-array antenna for hemispheric scan coverage," Trans. AP, AP-13, November, 1965, pp. 878-882.

22. J. L. Kmetzo, "An analytic approach to the coverage of a hemisphere by N planar phased arrays," Trans. AP, AP-15, May, 1967, pp. 367-371.

23. S. Edelberg and A. A. Oliner, "Mutual coupling effects in large antenna arrays: part II - compensation effects," IRE Trans. AP, 1960, p. 360.

24. E. G. Magill and H. A. Wheeler, "Wide-angle impedance matching of a planar array antenna by a dielectric sheet," Trans. AP, AP-14, January, 1966, pp. 49-53.

25. Wu and Galindo, "Surface wave effects on phased arrays of rectangular waveguide loaded with dielectric plugs," Trans. AP, May, 1968, pp. 358-360.

26. Hannan, Lerner, and Knittel, "Impedance matching a phased-array antenna over wide scan angles by connecting circuits," Trans. AP, AP-13, January, 1965, pp. 28-34.

27. N. Amitay, R. Pecina, and C. P. Wu, Bell Labs Mono. 5047, 1965.

28. N. Amitay, "Improvement of planar array match by compensation through contiguous element coupling," Trans. AP, AP-14, September, 1966, pp. 580-586.

29. L. I. Parad, "The input admittance to a slotted array with or without a dielectric sheet," Trans. AP, AP-15, March, 1967, pp. 302-304.

30. R. E. Collin, Field Theory of Guided Waves, McGraw-Hill, pp. 78-93.

31. R. F. Harrington, Time-Harmonic Electromagnetic Fields, McGraw-Hill, 1961.

32. C. P. Wu and V. Galindo, "Surface wave effects on phased arrays of rectangular waveguides loaded with dielectric plugs," Trans. AP, AP-16, May, 1968, pp. 358-360.

33. V. Galindo and C. P. Wu, "Dielectric loaded and covered rectangular waveguide phased arrays," BSTJ, vol. 47, January, 1968, pp. 93-116.

34. P. W. Hannan, "Proof that a phased-array antenna can be impedance matched for all scan angles," Radio Science, vol. 2, March, 1967, pp. 361-369.

35. N. Amitay, P. Butzien, and R. Heidt, "Match optimization of a two-port phased array antenna element," Trans. AP, AP-16, January, 1968, pp. 47-57.

36. Wu and Galindo, "Properties of an infinite phased array," 1965 URSI Fall Meeting Digest, pp. 71-72.

37. Wu and Galindo, "On the aysmptotic decay of coupling for infinite phased arrays," Proc. IEEE, November, 1968, pp. 1872-1880.

38. P. W. Hannan, "The ultimate decay of mutual coupling in a planar array antenna," Trans. AP, AP-14, March, 1966, pp. 246-248.

39. A. A. Oliner, "Surface wave effects and blindness in phased-array antennas," 1970 Phased-Array Antenna Symposium Digest, June, 1970, pp. 43-47.

40. M. J. Gans, "A general proof of Floquets' Theorem," IEEE Trans. AP, May, 1965, pp. 384-385.

41. J. Dudgeon, NASA contract report to be published.

42. H. A. Wheeler, "A systematic approach to the design of a radiator element for a phased array antenna," Proc. IEEE, vol. 56, November, 1968, pp. 1940-1951.

43. W. G. Scott and K. M. Soo Hoo, "A theorem on the polarization of null-free antennas," Trans. AP, vol. AP-14, No. 5, September, 1966, pp. 587-590.

44. W. G. Scott, "Rotating pseudo-patterns on the far field sphere of circularly polarized antennas," 1970 G-AP International Symposium Digest, September, 1970, pp. 288-295.